DEFORMATION AND FRACTURE MECHANISMS OF WASPALOY IN HOT TORSION

Sandor Fulop

A THESIS

in the

Faculty of Engineering

Presented in partial fulfilment of the requirements for
the Degree of Master of Engineering at
CONCORDIA UNIVERSITY
Montreal, Canada

April, 1976

TABLE OF CONTENTS

TABLE OF CONTENTS (CONT'D)

LIST OF FIGURES

LIST OF FIGURES (CONT'D)

LIST OF FIGURES(CONT'D

ACKNOWLEDGEMENTS

The author wishes to express his deep gratitude to his thesis supervisor, H. J. McQueen. Specific thanks are due to the staff in the Mechanical Engineering Department at Concordia University, to the staff in the Metallurgical Engineering Department at McGill University and to the staff of the Metallurgical Department at Pratt And Whitney Aircraft Of Canada Ltd.

ABSTRACT

DEFORMATION AND FRACTURE MECHANISM OF WASPALOY IN HOT TORSION

Sandor Fulop

Torsion tests were carried out on solid cylindrical test pieces of Waspaloy, using a servo-controlled closed-loop electrohydraulic torsion tester. The test program included strain rates between $0.03s^{-1}$ and $7.0s^{-1}$, temperatures ranging from room temperature to 1093°C (2000°F) and deformations up to strains of 45.

Increase of the testing temperature resulted in a decrease of the flow stress and generally an increase of the deformation to fracture. At a constant surface strain rate of $1.0s^{-1}$, cold working behaviour was observed at room temperature and at 649°C, warm working behaviour at 816°C and 899°C and hot working behaviour at and above 1010°C.

In the hot working region, the test pieces deformed to fracture showed a completely recrystallized structure and the flow curves showed a steady region after the work softening region. Recrystallization and cracking started after the peak of the flow curves. With 8.5 - 32 turns to fracture, cracking in the hot working region occurred by the formation of cavities on grain boundaries and at carbides, which coalesced into macroscopic cracks and final fracture. Increasing the strain rate in the hot working region resulted in an increase of the flow stress and decrease in the strain to fracture.

CHAPTER I

INTRODUCTION

1.1 Hot Working Studies

The purpose of the present work is to re-examine the information about the hot working of superalloys in light of the current theories of deformation and rupture with the aid of torsion test on Waspaloy over a range of strains, strain rates and temperatures.

The current theories on hot deformation mechanisms and their interaction with hot workability were derived from microstructural changes and from interactions of mechanical parameters, which were observed during experiments predominantly on pure metals and single phase alloys 1-31.

The relationship of these theories to Ni-base superalloys was reviewed in a paper by Fulop and McQueen[32], which is included as appendix 1; however the most pertinent aspects are repeated below.

Some of these studies included pure nickel and simple Ni-base alloys. During torsion tests on pure Ni and on Ni-Fe alloys, Luton and Tegart[26] concluded, that in the hot working region, the restoration mechanism was dynamic recrystallization. They established that during deformation cracks formed at triple points and at serrations on grain boundaries, and in the hot working region the growth of cracks was impeded as the grain boundaries moved away from them during dynamic recrystallization - attaining high ductility.

Sah, Richardson and Sellars [27] concluded that a model of continuous recrystallization was responsible for the shape of their flow curves during torsion experiments on pure nickel, however the flow curves in their paper did not quite extend into the steady region.

Shapiro and Dieter studied ductility and fracture of Inconel 600[29] and of pure nickel[31] in torsion tests with superimposed axial compression or tension stresses. Similar to the other workers, they found, that dynamic recrystallization was the restoration process in the hot working region. They also found that cracks formed on grain boundaries at the peak of the flow curve and the growth of cracks was arrested in the hot working region as the grain boundaries moved away from them during dynamic recrystallization.

Bailey studied hot workability of Waspaloy by rolling experiments[33], producing total reductions between 18% and 49% in several passes at finishing temperatures ranging from 960°C to 1060°C. In the analysis of the as-rolled microstructures Bailey describes the new grains as dynamically recrystallized grains. From the rolling schedule and from the amount of total strain involved in his experiments it is considered that the new grains were probably formed by static recrystallization in between passes and during cooling after deformation. Using a Gleeble high temperature testing machine, Bailey also studied hot workability of Unitemp HN (Ni-7% Cr-16.5 Mo)[34]. Taking the reduction of area after fracture as the measure of hot workability,

Bailey arrived at an optimum temperature range as a guide for hot pressing and rolling operations. In the description of the microstructure of the broken hot tensile specimens, Bailey concludes that the recrystallized grains are the product of dynamic recrystallization. The maximum reduction of area value shown in his paper was around 70%. From the amount of deformation and from the testing conditions it is considered that the final microstructure was produced partly by dynamic recrystallization during deformation and partly by metadynamic and static recrystallization after fracture.

The literature of hot working of superalloys includes: a.) studies by Muzyka[35], Donachie et al[36] and Reher et al[37] on the effect of second phases on the structure and properties of the material in the hot worked and final heat treated condition; b.) studies on the effect of second phases by Oblak et al[38], and of deformation rate on ductility during hot working by Cederblad and Grant[39]; and c.) experiments on thermomechanical strengthening by Hotzler et al[40], by Oblak and Owczarski[41] and by Kear et al[42].

The above hot workability studies include trials during industrial forming operations, experiments on simple shaped work pieces and laboratory tests on test pieces machined from the work pieces.

1.2 Mechanisms of Hot Deformation

Above about $0.6T_M$ of pure metals and single phase alloys, i.e. in the hot working region, dynamic restoration takes place simultaneously with the work hardening, maintaining sufficient ductility and allowing working without intermediate anneals. During hot working, the metals and alloys initially go through a work hardening region, in which there is a net increase of dislocations and increase of flow stress. After the initial work hardening region, the behaviour of metals and alloys falls into two categories, [9, 12, 18, 22, 24, 43] depending on the mechanism of restoration.

In metals and alloys with high stacking fault energy, where the dislocations have sufficient mobility, to climb and cross slip out of the slip plane, a continual generation and annihilation of dislocations maintains an equilibrium subgrain structure, similar to the second stage in creep. In the steady-state region, the moving dislocations are continually breaking up and rebuilding the sub-boundaries, and as a net result maintain an equilibrium subgrain size, dislocation density and the associated constant flow stress. In a given metal or alloy, high temperatures and lower deformation rates, which increase the amount of restoration, produce a larger subgrain size and lower dislocation density. The mechanism of maintaining an equilibrium subgrain structure is known as dynamic recovery.

In the metals and alloys with low stacking fault energy and with the resulting diminished dislocation mobility to leave the slip plane, the amount of recovery produced by annihilation of individual

dislocations is not sufficient to maintain a stable subgrain structure. Consequently, after a certain amount of deformation, sub-boundaries attain such high dislocation density that they become mobile high angle boundaries. As they migrate, they eliminate the dislocations, and leave behind a dislocation-free, recrystallized structure. After the initial work hardening region, there is a work softening region, in which the increasing amount of recrystallization reduces the flow stress. This is followed by a steady-state region, in which the continuous cycle of work hardening, recovery, recrystallization and work hardening maintains a dynamic equilibrium of dislocation density, grainsize and resultant flow stress. This latter restoration mechanism during hot work is known as dynamic recrystallization.

After the hot deformation is stopped, while the piece is held at working temperature and is cooling down from it, further restoration will take place by static recovery, metadynamic recrystallization and static recrystallization.

The hot workability of metals in industrial forming operations is related to the above mechanisms of dynamic restoration. They determine the flow stresses developed and the rate of crack propagation, thereby controlling the forming equipment's power requirements, and the amount of deformation, which can be applied in a single pass. Through their interaction with subsequent static recovery and static recrystallization - which happens when the metal remains hot, or is reheated after deformation - the dynamic processes also influence the structure and properties of metals at entrance of another forming operation, or at their end use.

1.3 Torsion Testing

The present work is concerned with the use of a torsion tester as a tool for hot deformation and particularly for hot workability studies on Waspaloy. Among the simple mechanical tools used for simulating hot working, in compression, or in tension where the test piece changes shape, the amount of available uniform deformation under constant strain rate is limited. Torsion tests can provide high-speed, constant strain rate testing, because high speed rotary motion is easy to produce and because the specimen does not change shape.

In a bar subjected to torsional moment M_T at one end, the twisting moment is resisted by shear stress τ set up in the cross section. For a cylindrical bar, the shear stress τ in the cross section, at a radial distance r from the centerline can be calculated from the following relation in the elastic range of deformation[44]:

$$\tau = \frac{M_T r}{J} = \frac{2 M_T r}{\pi a^4} \qquad \text{Where} \qquad (1)$$

τ = shear stress p.s.i.

M_T = torsional moment (torque) lb in; a = the outer radius of the bar

$$J = \frac{\pi (2a)^4}{32} = \text{polar moment of inertia}$$

Equation (1) can be derived by expressing the torsional moment M_T as the sum of incremental moment dM acting on a small surface element dA: (Fig. 1)

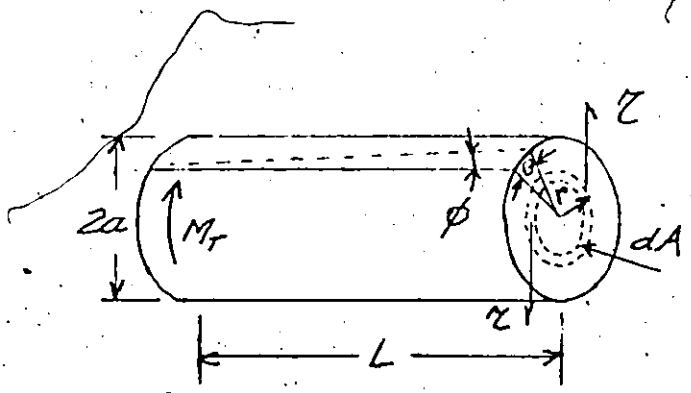

Fig. 1

$$M_T = \int dM = \int r\tau\, dA = 2\pi \int_{r=0}^{r=a} \tau r^2 dr \qquad (2)$$

The shear strain γ is given by

$$\gamma = \tan\phi = \frac{r\theta}{L} = r\theta' \qquad (3)$$

where $\theta' = \frac{\theta}{L}$

The shear stress τ is given by

$$\tau = G\gamma \qquad \text{where} \qquad (4)$$

$G =$ modulus of regidity

After the torsional yield strength has been exceeded, the shear stress distribution from center to surface is no longer linear, and equation (1) does not strictly apply. Nadai[45] has presented a method for calculating the shear stress in the plastic range from an actual torque-twist curve.

Assuming that the shear stress is a monotonously increasing function of the unit shear $\gamma = r\theta'$,

$$\tau = f(\gamma), \qquad (5)$$

he arrived at the following relation:

$$\tau_a = \frac{1}{2\pi a^3}\left(\theta' \frac{dM_T}{d\theta'} + 3M_T\right) \qquad (6)$$

where

τ_a = the max. shear stress in the outer fiber.

Fig. 2 illustrates the method of shear stress calculation from an available torque-twist curve.

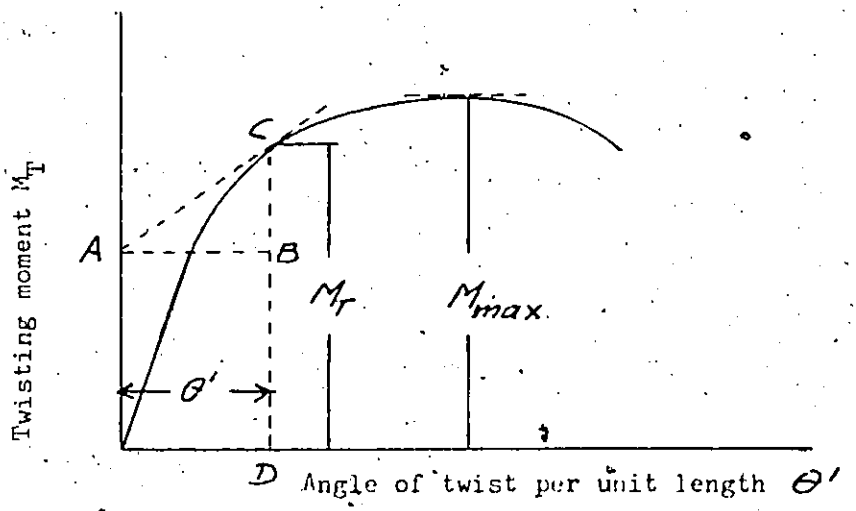

Fig. 2

Equation (6) can be rewritten in terms of the geometry of Fig. 2 as follows:

$$\tau_a = \frac{1}{2\pi a^3}\left(BC + 3CD\right) \qquad (7)$$

At the maximum value of torque, $dM_T / d\theta' = 0$.

Therefore, the ultimate torsional shear strength can be expressed by

$$\tau_u = \frac{3M_{max}}{2\pi a^3} \qquad (8)$$

For high temperatures and for high strain rates, the above

analysis was modified by Fields and Backhofen[46] to include the dependence of stress on strain rate. Considering that the torque is some function of both θ and $\dot{\theta}$, i.e. $M = \psi(\theta, \dot{\theta})$, equation (6) can be generalized. Then $dM/d\theta$ can be written as

$$\frac{dM}{d\theta} = \left(\frac{\partial M}{\partial \theta}\right)_{\dot{\theta}} + \left(\frac{\partial M}{\partial \dot{\theta}}\right)_{\theta} \times \frac{d\dot{\theta}}{d\theta} \qquad (9\text{-a})$$

Assuming that the radii remain constant, then

$$\gamma = r\theta', \quad \dot{\gamma} = r\dot{\theta}'; \quad \frac{\dot{\theta}'}{\theta'} = \frac{\dot{\gamma}}{\gamma} = \frac{\dot{\theta}}{\theta}; \quad \dot{\theta} = \frac{\theta\dot{\gamma}}{\gamma}; \quad \frac{d\dot{\theta}}{d\theta} = \frac{\dot{\gamma}}{\gamma} = \frac{\dot{\theta}}{\theta}$$

Equation (9a) becomes then

$$\frac{dM}{d\theta} = \left(\frac{\partial M}{\partial \theta}\right)_{\dot{\theta}} + \left(\frac{\partial M}{\partial \dot{\theta}}\right)_{\theta} \times \frac{\dot{\theta}}{\theta} \qquad (9\text{-b})$$

The terms of equation (9-b) can be evaluated, by using the experimental observation, that the logarithmic plots of M versus θ at a constant $\dot{\theta}$ and of M versus $\dot{\theta}$ at a constant θ are straight lines. The The slopes of these plots are then equivalent to the strain hardening exponent (n) and rate sensitivity exponent (m).

Thus if $M = M_0\theta^n$ for const. $\dot{\theta}$, and $M = M_1\dot{\theta}^m$ for const. θ, then $\left(\frac{\partial M}{\partial \theta}\right)_{\dot{\theta}} = \frac{nM}{\theta}$; and $\left(\frac{\partial M}{\partial \dot{\theta}}\right)_{\theta} = \frac{mM}{\dot{\theta}}$, giving

$$\frac{dM}{d\theta} = \frac{M}{\theta}(n+m), \quad \text{thus}$$

$$\tau_a = \frac{M}{2\pi\alpha^3}(3+n+m) \qquad (9\text{-c})$$

The state of stress on the surface of a bar subjected to torsion is illustrated on Fig. 3[44]. The max. shear stress occurs on two mutually

perpendicular planes, perpendicular to the longitudinal axis xx, and parallel with it. The principal stresses σ_1 and σ_3 make an angle 45° with the longitudinal axis and are equal in magnitude to the shear stress. σ_1 is a tensile stress and σ_3 is an equal compressive stress. The intermediate stress σ_2 is zero.

The strains and the above corresponding stresses in torsion are given by the following relations[44]:

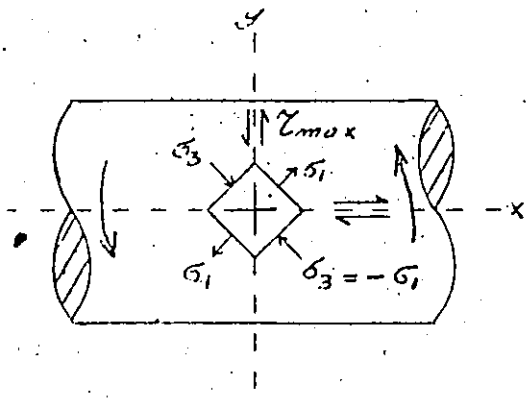

Fig. 3

$$\sigma_1 = -\sigma_3 \; ; \quad \sigma_2 = 0 \tag{10}$$

$$\tau_{max} = \frac{\sigma_1 - \sigma_3}{2} = \sigma_1 \tag{11}$$

$$\varepsilon_{max} = \varepsilon_1 = -\varepsilon_3 \; ; \; \varepsilon_2 = 0 \tag{12}$$

$$\gamma_{max} = \varepsilon_1 - \varepsilon_3 = 2\varepsilon_1 \tag{13}$$

The equivalent stress $\bar{\sigma}$ and equivalent strain $\bar{\varepsilon}$ are given as

$$\bar{\sigma} = \sqrt{3}\,\sigma_1 \tag{14}$$

$$\bar{\varepsilon} = \frac{2\varepsilon_1}{\sqrt{3}} = \frac{\gamma}{\sqrt{3}} \tag{15}$$

In general, ductile materials fail in torsion by shear along a plane of max. shear stress, usually the one nearest to the longitudinal axis. Brittle materials fail along a plane perpendicular to the direction of maximum tensile stress resulting in the "wolf's ear" shape.

CHAPTER II

EXPERIMENTAL PROCEDURE

2.1 Test Program and Test Material

Constant strain rate torsion tests were carried out on Waspaloy, at temperatures between room temperature and 1093°C (2000°F) and equivalent surface strain rates between $0.03s^{-1}$ and $7.0s^{-1}$. The test pieces were solid cylinders with a test section 25.4 mm (1") long and 6.25 mm (0.25") diameter. To reduce the temperature gradient along the test length, transition shoulders of intermediate diameter were provided on both ends between the test length and the gripping ends. (At 1038°C, the middle of the gauge length was 3-4°C hotter than the ends).

In one series of tests, the test pieces were deformed to fracture at a constant surface strain rate of $1.0s^{-1}$ at temperatures between room temperature and 1093°C to identify cold-, warm- and hot deformation and fracture behaviour. In a second series of tests, the specimens were deformed at 1038°C (1900°F) with surface strain rates between $0.03s^{-1}$ and $7.0s^{-1}$ to study the effect of strain rate on ductility. In a third group, the test pieces were deformed at 1038°C, with a strain rate of $0.1s^{-1}$, to different amounts of predetermined strain between $\bar{\varepsilon} = 0.15$ and .45, then quenched to study recrystallization and fracture initiation and propagation. In addition, a few more tests were run at testing temperatures of 1010°C, 1038°C and 1065°C, with strain rates of $0.2s^{-1}$, $1.0s^{-1}$ and $2.0s^{-1}$ to provide

additional data for determining the depencence of flow stress on temperature and on strain rate.

The material used for the experiments was a 16mm hexagonal hot rolled barstock (Carpenter heat 85516). The test material was annealed at 1120°C (2050°F) and air cooled to coarsen the grain size in order to facilitate the observation of the initial stages of recrystallization and fracture initiation. This annealing treatment produced a grain size of ASTM 1-2 and dissolved the γ' ($Ni_3(Al,Ti)$ and $M_{23}C_6$ carbides and some of the MC carbides. The subsequent air cooling precipitated some fine γ' and carbides. The times of 3-5 minutes for heating up and of 5 minutes holding at testing temperatures before deformation caused further precipitation of γ' and $M_{23}C_6$ carbides in specimens tested at warm working temperatures. Re-solution of γ' and $M_{23}C_6$ carbides, and precipitation of MC carbides occurred at the high end of the temperature range. With the 3.1% Ti and 1.6% Al content of the test material, the estimated γ' solvus was $\approx$ 1050°C ($\approx$ 1925°F).

2.2 Testing System and Testing Procedure

A servo-controlled closed loop torsion testing system was built for these experiments and for further hot deformation studies[47]. (Figs. 4-1 and 4-2). On the torsional frame (Fig. 5-1) the test pieces were held by superalloy loading members, and one end of the test piece was twisted by a measured amount by a hydraulic motor (Fig. 5-2), while the other end was held fixed by a reaction torque cell (Fig. 5-3).

During the tests the longitudinal stresses were not controlled. For tests carried to fracture, both gripping ends of the test pieces were threaded and a constant test piece length was maintained. The test pieces used in the interrupted tests were threaded on one end and on the other had a rectangular section which slipped into a slot in the loading bar to allow removal without accidental straining. (Fig. 5-4).

The test pieces were heated by a water cooled radiant furnace - controlled by a combined temperature/power controller. To reduce the thermal gradient along the test piece's gauge length, a 20mm wide strip of the parabolic mirror was shaded by carbon black. The controlling thermocouple extends into the test piece shoulder through the reaction bar. The furnace is mounted on a sliding stand with longitudinal freedom of movement, to assist assembling and disassembling of the sample and loading members (Fig. 5-5). For oxidation protection of the test piece, the furnace chamber can be flushed with a flow of argon gas, or an enclosing silica tube is provided, in which a vacuum or argon atmosphere can be maintained. To quench the test pieces for structural studies, particularly in interrupted tests, the tube was flooded with water, but in other cases the test pieces were cooled by a flow of gas.

The displacement of the motor is controlled by a closed-loop "MTS" control system (Fig. 5-6). The rotary displacement is measured by a dual gang potentiometer, which provides the feedback signal to the

controller. The torsion tester can be operated on either rotary displacement or torque feed back mode. The former was used for the present experiments. During test, torque and angular displacement were recorded by a Hewlett Packard X-Y recorder, or by a Hewlett Packard high speed galvanometric recorder.

The torsion machine is capable of applying a maximum of 100 revolutions of twist at velocities up to 15 revolutions/sec., with a max. torque of 110 Nm. With the 25.4 mm by 6.25 mm test pieces used in these experiments, these parameters correspond to a maximum shear strain of 80, shear strain rate of $12s^{-1}$, and shear stress of 1800 MPa. With the shorter test pieces, 2:1 length to radius ratio, which avoids serious end effects, the present machine could reach a surface strain rate of $48s^{-1}$.

Before the experiments, a correlation between the controlling thermocouple and the gauge length temperature was established by temperature surveys run with external thermocouples embedded into the test length. Similarly, the output of the reaction torque cell was calibrated with a lever system and known weights.

Based on the initial calibration, the actual experimental values of temperature and torque were within $\pm$ 1% of the recorded values.

CHAPTER III

TEST RESULTS

3.1 Flow Curves

During the present experiments, from the recorded torque and twist data, the true surface shear stress and equivalent surface strain values were calculated - using equations (9c) and (15) respectively. In equation (9c) the value of m was taken as 0.12 after Rossard and that of n was taken as zero, although this is strictly valid only at the peak and during steady state. The recorded torque twist curves and the calculated true surface stress and equivalent surface strain values are presented in Figs. 6-1, 6-2 and 6-3.

3.2 Flow Stress-Temperature-Strain Rate Relations

For three temperatures (1010°C, 1038°C and 1065°C) in the hot working range, a plot of $\ln \dot{\varepsilon}$ versus flow stress σ resulted in three parallel lines shown in Fig. 7-1. (Because at higher strain rates the flow stress was slightly decreasing with increasing strain in the steady region, the value of flow stress was taken after the end of the work softening region at about 7 turns for each of the tests represented in the plot). The fit to a straight line indicates that the following equation is obeyed:

$$\dot{\varepsilon}_T = A \exp(\beta \sigma) \qquad (16)$$

β was found to be 6.72×10^{-4} psi^{-1} from the slope of the lines, according to the following relation

$$\frac{d(\ln \dot{\varepsilon}_T)}{d\sigma} = \beta \qquad (17)$$

The temperature dependence was found to obey an Arrhenius relationship of the type:

$$\dot{\varepsilon} = B \exp(\beta\sigma) \exp\left(\frac{-\Delta H}{RT}\right) \qquad (18)$$

by taking the logarithmic values,

$$\ln \dot{\varepsilon} = \ln B + \beta\sigma - \frac{\Delta H}{RT} \qquad (19)$$

and differentiating at a constant $\dot{\varepsilon}$ value, the activation energy is given:

$$\left(\frac{\partial(\beta\sigma)}{\partial 1/T}\right)_{\dot{\varepsilon}} R = \Delta H \qquad (20)$$

Which is the slope of the $\beta\sigma R$ versus 1/T plots shown for the three different strain rates ($\dot{\varepsilon}$ =2.0s^{-1}, 1.0s^{-1} and 0.2s^{-1}) on Fig. 7-2. ΔH was found to be 98 Kcal/mol.

3.3 Macroscopy and Metallography

After deformation the test pieces were macroscopically examined at magnifications between 5X and 50X. The results of the macrographic analysis are shown in Figures 8-1 to 8-4. Fig. 8-1 (a) and (b) are

undeformed and Fig. 8-1 (c), (d) and (e) illustrate deformed but unbroken specimens. Specimens fractured over a range of temperatures from 816°c to 1093°C are illustrated in Fig. 8-2 at normal size and in Fig. 8-3 and 8-4 at X5 magnification. Fig. 8-4 (c) and (d) illustrate samples deformed at 1038°C, one to the fracture strain, and the other to a strain just less.

After macroscopic examination longitudinal diametral sections were cut from the deformed test pieces for metallographic examination. The test pieces were ground on carborundum papers and mechanically polished with 6 micron and 1 micron diamond. After polishing, the specimens were examined unetched to observe cracks and then they were etched in Fry's reagent to study deformation, recrystallization, fracture initiation and propagation. The micrographs of the longitudinal diametral sections are presented in Figs. 9 to 27, in all cases oriented with the longitudinal axis horizontal.

CHAPTER IV

DISCUSSION OF RESULTS

4.1 Flow Curves

In Fig. 6-1 it is seen that with the increase of testing temperature the test pieces showed a decrease of flow stress and an increase in the available deformation before fracture. The test pieces deformed at 25°C and at 649°C broke at the maximum of the torque/twist curve, indicating a cold working behaviour. The test pieces deformed at 816°C, 899°C, 954°C and 982°C showed a broad peak on the torque/twist curve followed by a decrease of flow stress before fracture, indicating a warm working behaviour. During the tests run at 1010°C, 1038°C, 1065°C and 1093°C, the flow curves showed work hardening to a peak followed by work softening to a steady region in which the flow stress changed very little with additional deformation; this is typical of metals undergoing dynamic recrystallization during hot deformation.

4.2 Macroscopic Examination

The test pieces all broke on a surface at right angles to the longitudinal axis (one of the two planes of max. shear). The test pieces tested between 25°C and 899°C broke in a clear cut shear mode, producing a flat fracture surface with no distortion of the original cylindrical geometry (Fig. 8-2a). At and above 954°C, the fracture surfaces were not flat, as a result of cracks on more than one adjacent plane joining up to produce the fracture and there was a local swelling of the diameter in the fracture zone.

At all temperatures the test piece's surface showed spiral markings, corresponding to the number of twists. (Figs. 8-1 and 8-2). The surface of the test pieces deformed at 25°C and at 649°C showed orange peel markings at low magnifications as a result of the large grain size (Fig. 8-3) and slip bands at higher magnifications (X50). At 649°C the orange peel markings and slip bands were less pronounced as the slip bands were more wavy. Above 649°C, up to 954°C, the deformation markings were still in evidence, in decreasing intensity with increase of temperature. At and above 954°C, the test pieces showed spiral fissures or extrusion/intrusion markings near the fracture region, however this region enlarged as the temperature increased, spreading into the whole gauge length at and above 1038°C. The intensity (depth) of the intrusions/extrusions increase with increasing temperature and increasing strain. At and above 1010°C, the test pieces showed surface irregularities superimposed on the extrusions/intrusions. The irregularities spread into the whole gauge length as the temperature increased to 1093°C. These irregularities appeared as globular expulsions at higher magnifications (X50). Careful examination of the extrusion/intrusion region showed, that they were generally longer, deeper and more open in the fracture region than elsewhere. The cracks at 25°C and 649°C were fairly narrow. At 649°C and 1093°C the cracks were long (some ran circumferentially all around). At 816°C, 899°C at 954°C, the circumferential cracks were shorter and more open, and in addition to the circumferential cracks, there were present some longitudinal cracks and some at about 45° to the axis.

There was an abundance of cracks on the surface of test pieces fractured at 816°C and at 899°C. At all temperatures, there was a concentration of deformation in the fracture region, as evidenced by the deformation markings, extrusions/intrusions and by the larger amount and larger size of cracks. In all the tests, the deformation extended part way into the filet at the ends of the test piece.

4.3 Metallography of Diametral Sections

All the test pieces deformed to fracture showed signs of deformation in the whole gauge length and in the whole gauge diameter. The amount of deformation decreased going from the surface towards center. In the analytical treatment of torsion testing stresses and strains are calculated in terms of pure shear of a bar subjected to a twisting moment and the shear strain γ is zero at r=0 (Equation 3). Due to the Taylor's effect in polycrystalline specimens, the centerline region also becomes strained. The deformation was most intensive near the fracture and diminished towards the shoulders extending part way into the filet region.

The test pieces fractured at room temperature (25°C), exhibited deformation in the form of distorted grains, serration of grain boundaries and pronounced slip bands inside the grains. The slip bands were sharply defined and straight, indicating a predominantly planar slip. In addition to the "homogeneous" deformation of grains, there were transverse deformation bands going through several grains at and near the outer diameter (Figs. 9a, 9b). There were transverse cracks,

extending from the surface to a depth of 0.003". Most of the cracks, including the largest ones in the fracture zone, were in the transverse deformation bands at and near the outer surface (Fig. 9b). The main cracks were transgranular. On the longitudinal grain boundaries there were numerous small cracks at ledges, where the deformation bands, crossed grain boundaries (Fig. 9b). There were also some grain boundary cracks, possibly associated with transverse grain boundary sliding. (Fig. 9c). Within the grains, there were a few cracks associated with inclusions.

In the test piece fractured at 649°C, (Figs. 10a-10c) the slip bands and deformation bands were much less pronounced and fewer than in the sample deformed at 25°C. Although this was partly due to the lower breaking strain, the weak deformation markings at the outer diameter, where the strain is the highest, indicate that deformation was more diffuse with cross-slip of screw dislocations and partial recovery.

The surface exhibits transverse cracks along the whole gauge length to a depth of about 0.010". All these are transgranular. Most of the cracks, including the largest ones in the fracture zone, are in transverse bands at and near the surface (Figs. 10a, 10b and 10c). There are also numerous small cracks at ledges where the deformation bands cross longitudinal boundaries (Fig. 10b) and at twin plates (Fig. 10c). There are some cracks on transverse boundaries as well at ledges at the ends of twin plates.

Nucleation of cracks in zones of concentrated deformation bands observed at both 25°C and 649°C is explained by a mechanism proposed by Tetelman[48]. Crack nucleation occurs when the concentrated tensile stress at the tip of a blocked edge dislocation band equals the theoretical cohesive stress. This crack nucleation occurs at a shear stress τ_N as the result of the pile up of dislocations.

According to the following relation:

$$(\tau_N - \tau_i)(n b) = 2\gamma_m \qquad (21)$$

crack will nucleate when the work $\tau_N nb$ done by the applied stress τ_N in producing nb displacement, equals to the work done against the frictional forces $\tau_i nb$ plus the work $2\gamma_m$ to make the new fracture surface, where τ_i is the frictional stress and γ_m is the surface energy, including the plastic work done around the crack tip.

The samples fractured at 816°C (Figs. 11a, b&c) and 899°C (Figs. 12a, b&c), show little or no evidence of slip bands respectively. At both temperatures there is still some evidence of localized transverse deformation bands.

Both samples show transverse cracks in the whole gauge length between the surface and a maximum depth of about 0.020", however most of the cracks are not connected to the surface. In addition, there are cracks present in the whole cross section, right down to the centerline. At

and near the fracture most of the cracks are on transverse twin boundaries and at some transverse grain boundaries. (Figs. 11b, 11c, 12b and 12c). There are cracks on longitudinal twin boundaries (Figs. 11c, 12c), on oblique twin boundaries and grain boundaries (Figs. 11b, 11c, 12b and 12c), and on grain boundary triple conjunction (Fig. 12b). The cracks in the sample fractured at 899°C were more open. The major portion of cracking damage leading to fracture in the warm working region (816°C and 899°C) was due to twin and grain boundary cracks in the transverse shear direction. The contribution from cracks in the deformation bands is much less than at lower temperatures because the pile ups are much less as a result of recovery.

At test temperatures of 954°C and 982°C, the fractured test pieces showed pronounced recrystallization near the fracture zone. The amount of recrystallization decreased moving away from the fracture zone towards the shoulder and towards the centerline. At 954°C, the recrystallization was nearly complete at the fracture (Figs. 13a and b), while at 982°C it was complete (Figs. 14a and b). In the partially recrystallized areas, recrystallization occurred on grain boundaries and on twin boundaries (Figs. 13c and 14c).

The cracks at 954°C are confined mainly to the fracture region (Figs. 13a, b and c). There are transverse grain boundary and twin boundary cracks, some of them wedge shaped. Away from the fracture zone there are only a few cracks present - again on grain boundaries and at twin boundaries. The cracks and recrystallization extend to about mid-

radius away from the fracture. At 982°C, extrusions/intrusions occur on the surface in the fracture zone. The cracks are mainly confined to the fracture zone (Figs. 14a and b), and are mainly of the grain boundary cavity (pore) type (Fig. 14b). In the centerline at the fracture, the cracks are mainly at carbide inclusions. Away from the fracture there are a few cracks on transverse grain and twin boundaries (Fig. 14c). For the strain rate of $1.0s^{-1}$, these two temperatures (954°C and 982°C) represent transition from the warm to the hot working range.

The test pieces deformed to fracture at temperatures of 1010°C, 1038°C and 1093°C, show dynamic recrystallization in the whole gauge length, in conformance with the work softening and steady regions on the flow curves. The whole cross section is recrystallized and recrystallization extends halfway into the radius at the gauge length ends. With the increase of temperature there was an increase of the grain size and a decrease of the flow stress. The surface shows extrusion/intrusion markings.

Cracking and fracture at these temperatures occurred by the formation of pores at grain boundaries and carbides and the coalescence of these pores into macroscopic cracks. (Figs. 15-18). The pores and "cracks" are concentrated in the fracture region and their numbers decrease going towards the shoulders (Figs. 17d, 17e and 17f), and decreases going towards the centerline (Figs. 17d, 17b and 17c). At the centerline some of the pores and cracks are associated with carbide inclusions (Figs. 15c and 16c). Apart from the centerline, there is no direct

evidence of the pores being associated with carbides. In the fracture zone the scalloped shape of the "cracks" indicate, that they were formed by coalescence of cavities (Figs. 16a, 16b, 17a, 17b, 17c). In the fracture zone the pores and cracks are both on current grain boundaries and inside grains (Figs. 16a, 16b, 17a, 17b and 17c). Away from the fracture zone, the pores are on grain boundaries and at carbides (15c and 16c). From the above observations, it is postulated, that the pores initially form on grain boundaries and at carbides, however they stop growing, when the grain boundaries move away from them during dynamic recrystallization, and resume growth again only when a moving boundary dwells at the previously formed pore or crack. The test piece fractured at the highest temperature (1093°C) shows longer and narrower coalesced pores (Figs. 18b and c), than samples deformed lower in the hot working range (1010°C, 1038°C and 1065°C).

As the recorded torque/twist curves at 1038°C indicate (Fig. 6-2), the increase in strain rate from $3x10^{-2}s^{-1}$ to $7.0s^{-1}$ caused the ductility to decrease, flow stresses to increase. The test pieces twisted at the lower strain rates ($0.03s^{-1}$, $0.1s^{-1}$, $0.2s^{-1}$) showed a true steady state region of constant flow stress after the work softening region and exhibited good ductility, i.e., did not break after 50 turns. The specimens twisted at the medium strain rate range ($0.4s^{-1}$, $0.7s^{-1}$, $1.0s^{-1}$ $2.0s^{-1}$) gave good ductility, and after a peak, a softening region, in which the flow stress slowly decreased until fracture. This diminishing flow stress is thought to be due partly to adiabatic heating and partly due to decrease of cross section by the accumulative damage

by the formation of pores (cracks). The test pieces deformed at the highest strain rate, $7.0s^{-1}$ broke after the work softening region without a steady state region and gave a lower ductility, (5.3 turns to fracture).

At all these strain rates, after deformation the test pieces showed a dynamically recrystallized structure and the cracks formed by coalescence of pores.

Near the fracture some of the cracks and pores were connected to the intrusions at the surface (Figs. 16a, 17a and 18a), however there is no direct evidence showing that the final fracture occurred by an intrusion penetrating into the body of the samples. The evidence presented previously on the photomicrographs indicated that final fracture occurred by coalescence of the pores into macroscopic cracks.

During one of the tests at the highest strain rate ($7.s^{-1}$), the deformation was stopped on the falling part of the flow curve before fracture at a total twist of 5 turns. Macroscopic examination of this test piece after deformation showed a localized region of concentrated deformation, judged by the spiral line distribution along the gauge length. Metallographic examination of this more deformed region showed larger concentration of pores, than the rest of the gauge length. This localized heavier deformation is considered to be the result of the weakening which accompanies pore formation. Photomicrographs of this region (Figs. 19a, b and c) nicely illustrate the

effect of strain and strain rate on recrystallization and pore formation, i.e., the annulus at larger radius has the finest grain size and the largest number of pores and the centerline region has the coarsest grain size and the smallest number of pores.

The relationship of different interruption strains to the characteristic features of the flow curve are shown on Fig. 6.3.

The sample twisted to $\bar{\varepsilon} = 0.15$ (0.3 turns) just before the peak showed no recrystallization (Figs. 20a and b). At $\bar{\varepsilon} = 0.30$, there was a small amount of recrystallization in the sample twisted to $\bar{\varepsilon} = 0.45$, which falls in the beginning of the work softening region of the curve. The recrystallization occurred on the original grain boundaries and twin boundaries and was confined to the surface region (Fig. 21a). Deformation of the original grains was evidenced in the central region by the serration of grain boundaries and bending of twin boundaries without recrystallization (Fig. 21b). The sample twisted to $\bar{\varepsilon} = 0.75$ showed more recrystallization in the outer radius - with the original grains still very much in evidence (Fig. 22a). The centerline region of this sample showed initial stages of recrystallization (Fig. 22b). The sample twisted to $\bar{\varepsilon} = 2.3$ (which is just less than the end of the work softening region at $\bar{\varepsilon} \approx 3.2$) showed almost complete recrystallization at the outer radius region (Fig. 23a), and appreciable amounts of recrystallization in the centerline region on the grain boundaries and twin boundaries of the original grains (Fig. 23b). The sample

twisted into the steady state regime, $\bar{\varepsilon} = 4.5$ showed complete recrystallization on the whole cross section (Figs. 24a and b). After further deformation in the steady state region to $\bar{\varepsilon} = 22.5$ (Figs. 25a and b), the grain structure is the same as at $\bar{\varepsilon} = 4.5$. Evidently dynamic recrystallization maintained the grain size constant in the steady state regime.

Pore formation was first noticed in the sample twisted beyond the peak of the flow curve ($\bar{\varepsilon} = 0.75$) as shown in Fig. 26a. This observation is in agreement with E. Shapiro and G. E. Dieter's finding on Inconel 600[29]. A sample deformed into the work softening range (5 turns, $\bar{\varepsilon} = 2.3$) showed appreciable amounts of pores, especially at and near the outer surface region (Fig. 27a). Away from the outer region a noticeable number of pores are formed as extension of the cracks at the carbide particles or by decohesion at the carbide - matrix interface (Figs. 27b and 27c). Comparing these latter photomicrographs of the sample deformed at surface strain rate of $0.1s^{-1}$ with the sample deformed the same amount with a surface strain rate of $7.0s^{-1}$, (Figs. 19a, b and c), it becomes apparent, that throughout the strain rate range examined at 1038°C, (in the hot working range) the cracks were initiated by the same mechanisms.

In the steady state region of the samples deformed with the slow strain rate, $\dot{\varepsilon} = 0.1s^{-1}$, there was no increase in pore formation with increasing amounts of strain. At this strain rate, the fracture strain exceeded 50 turns.

SUMMARY

1.)

In a series of torsion tests, at a constant strain rate $\dot{\varepsilon} = 1.0s^{-1}$, increase in the testing temperature resulted in a decrease in flow stress and generally an increase of the deformation to fracture. Cold working behaviour was observed at testing temperatures of 25°C and 649°C. At 25°C, the sample developed heavy slip bands in the grains and localized heavy deformation bands in the plane of maximum shear stress perpendicular to the axis. Cracking and fracture took place in these transverse deformation bands. At 649°C, the deformation in the grains took place in a more diffuse manner, but cracking and fracture still occurred in transverse deformation bands. At 816°C and 899°C, warm working behaviour was observed. Partial recovery took place and cracking developed due to sliding of grain boundaries and incoherent twin boundaries leading to a fracture in the plane normal to the axis. Temperatures of 954°C and 982°C, represented a transition between warm working and hot working. The sample at 954°C cracked and fractured in the same manner as those in the warm working range, but underwent some recrystallization, mainly in the fracture zone. At 982°C, fracture occurred by formation and coalescence of pores, similar to the samples in the hot working region and appreciable amounts of recrystallization took place. However away from the fracture, cracks due to boundary sliding were observed. In the hot working temperature range, 1010°C to 1093°C, the samples were completely dynamically recrystallized and the flow curves showed a steady state regime after the work softening region consistent with

dynamic recrystallization. With 8.5 - 32 turns to fracture, cracking occurred by the formation of cavities on grain boundaries and at carbides, which coalesced into macroscopic cracks and final fracture on the plane of maximum shear stress transverse to the axis.

2.)

Increasing the strain rate in the hot working range (1038°C) resulted in an increase of the flow stress and decrease in the strain to fracture. At the two lowest strain rates ($0.03s^{-1}$ and $0.1s^{-1}$) the samples did not break before 50 turns. At the highest strain rate, $7.0s^{-1}$ the samples broke at 5.3 turns. All these samples were dynamically recrystallized after deformation and cracks formed by coalescence of pores.

3.)

Interrupted tests carried out at 1038°C, at a surface strain rate of $0.1s^{-1}$, indicated, that dynamic recrystallization and cavity formation started at the maximum of the flow curve and recrystallization became complete by the end of the work softening stage. In the steady state regime continual dynamic recrystallization maintained a constant grain structure.

4.)

The interdependence of strain rate, flow stress and temperature was found to obey an Arrhenius relationship of the type:

$$\dot{\varepsilon} = B \exp(\beta\sigma) \exp\left(\frac{-\Delta H}{RT}\right)$$

The activation energy was calculated to be 98 kcal mol^{-1}.

Fig.4-1. Hot Torsion Machine with Deformation and Environment Control Consoles.

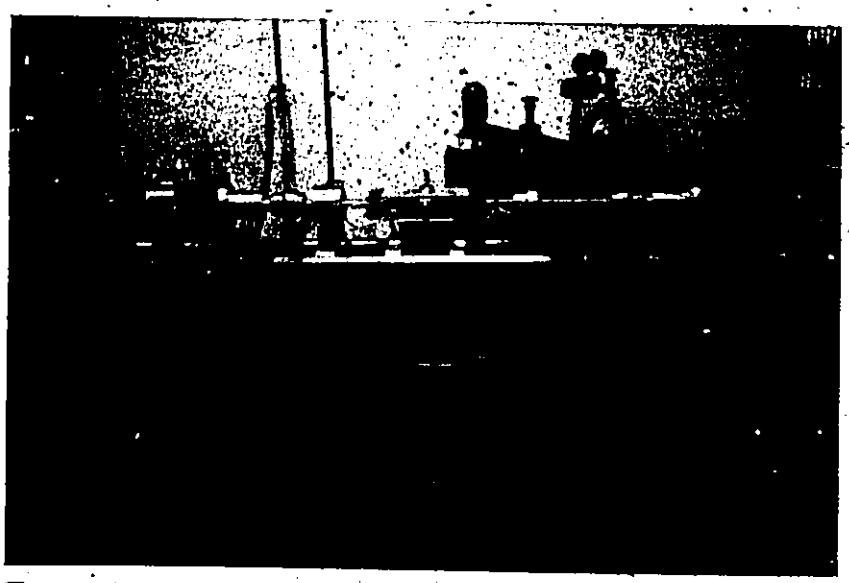

Fig.4-2. Servo-Controlled Hot Torsion Machine

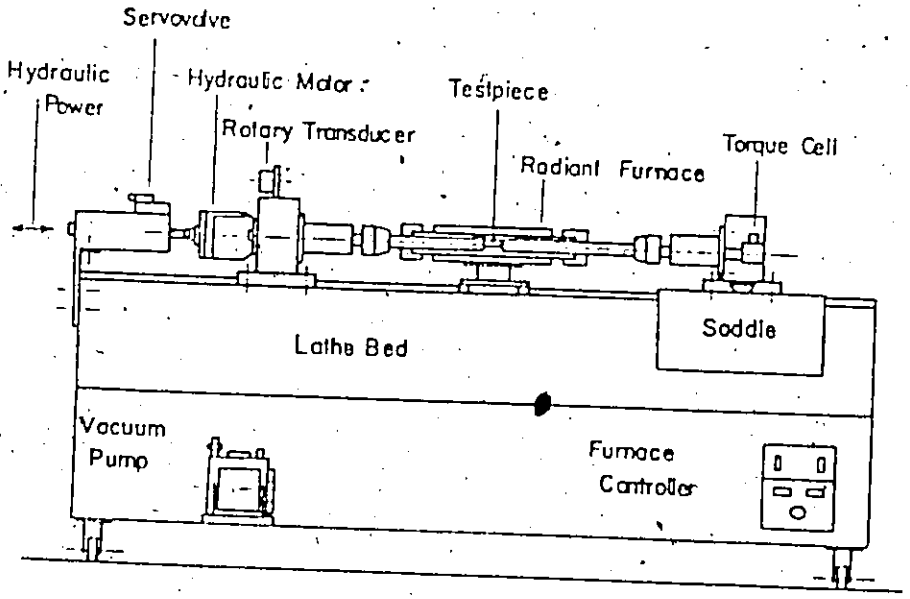

Servo-controlled Hydraulic Torsion Machine

Fig. 5-1

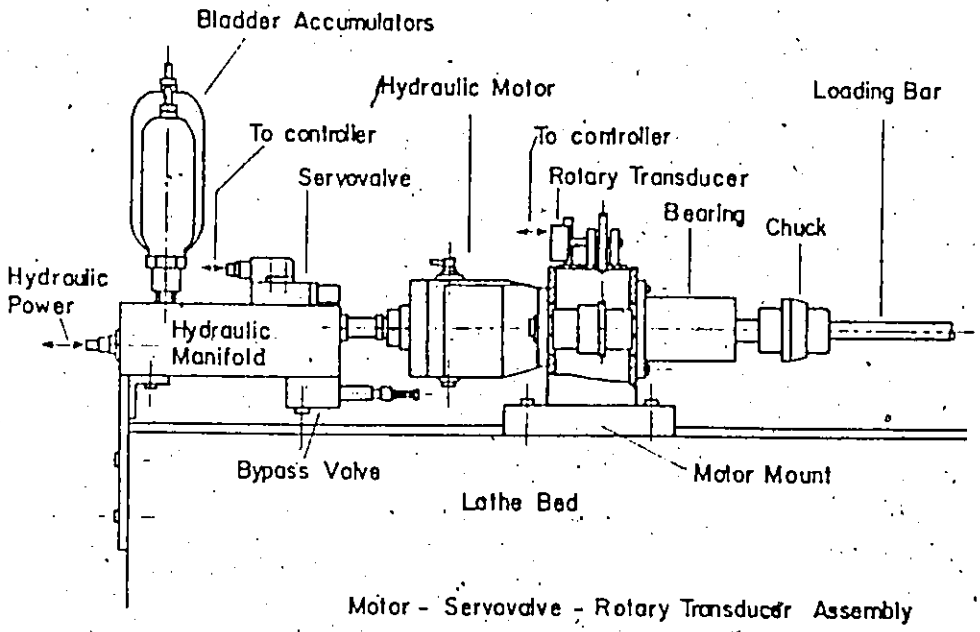

Motor - Servovalve - Rotary Transducer Assembly

Fig. 5-2

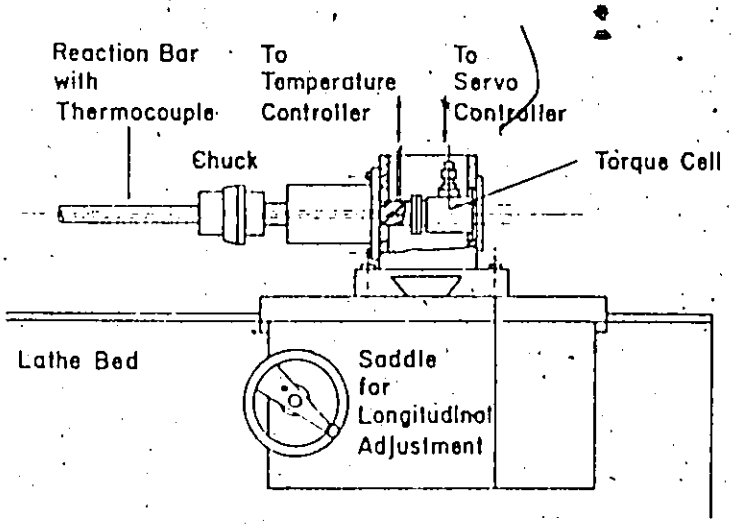

Torque Cell Assembly

Fig. 5-3

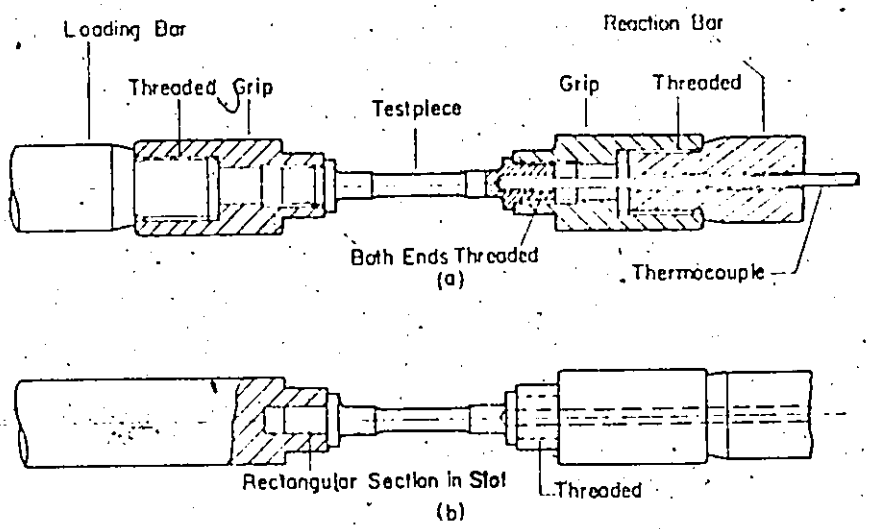

Testpiece and Grip Designs

Fig. 5-4

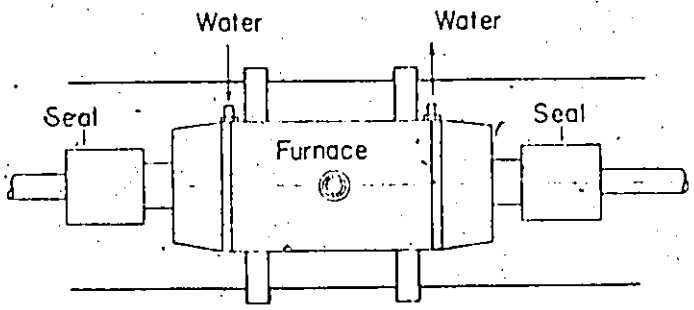

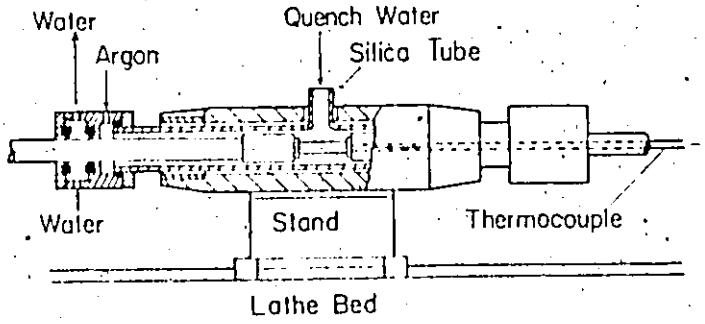

Furnace with Protective Environment

Fig. 5-5

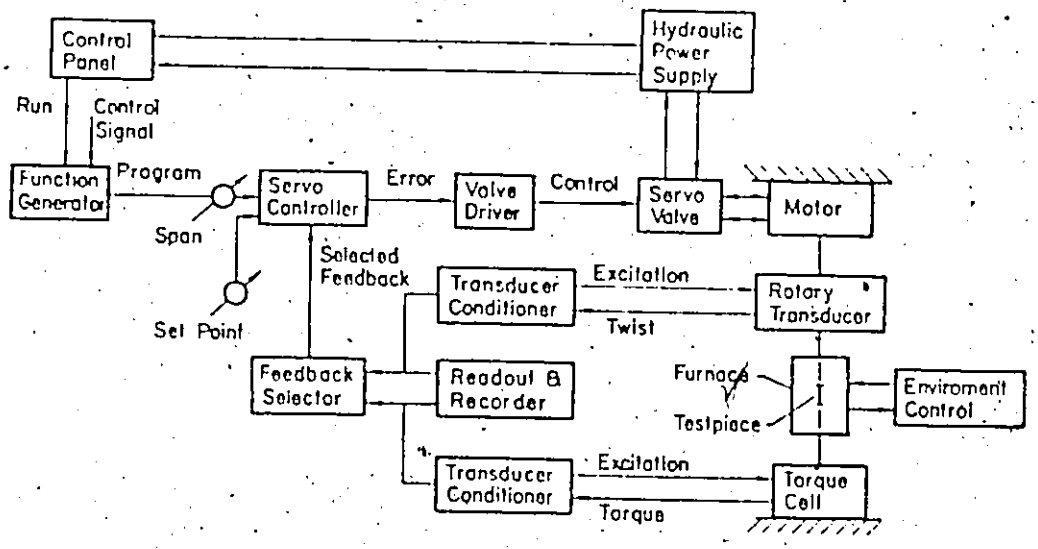

The Control System.

Fig. 5-6

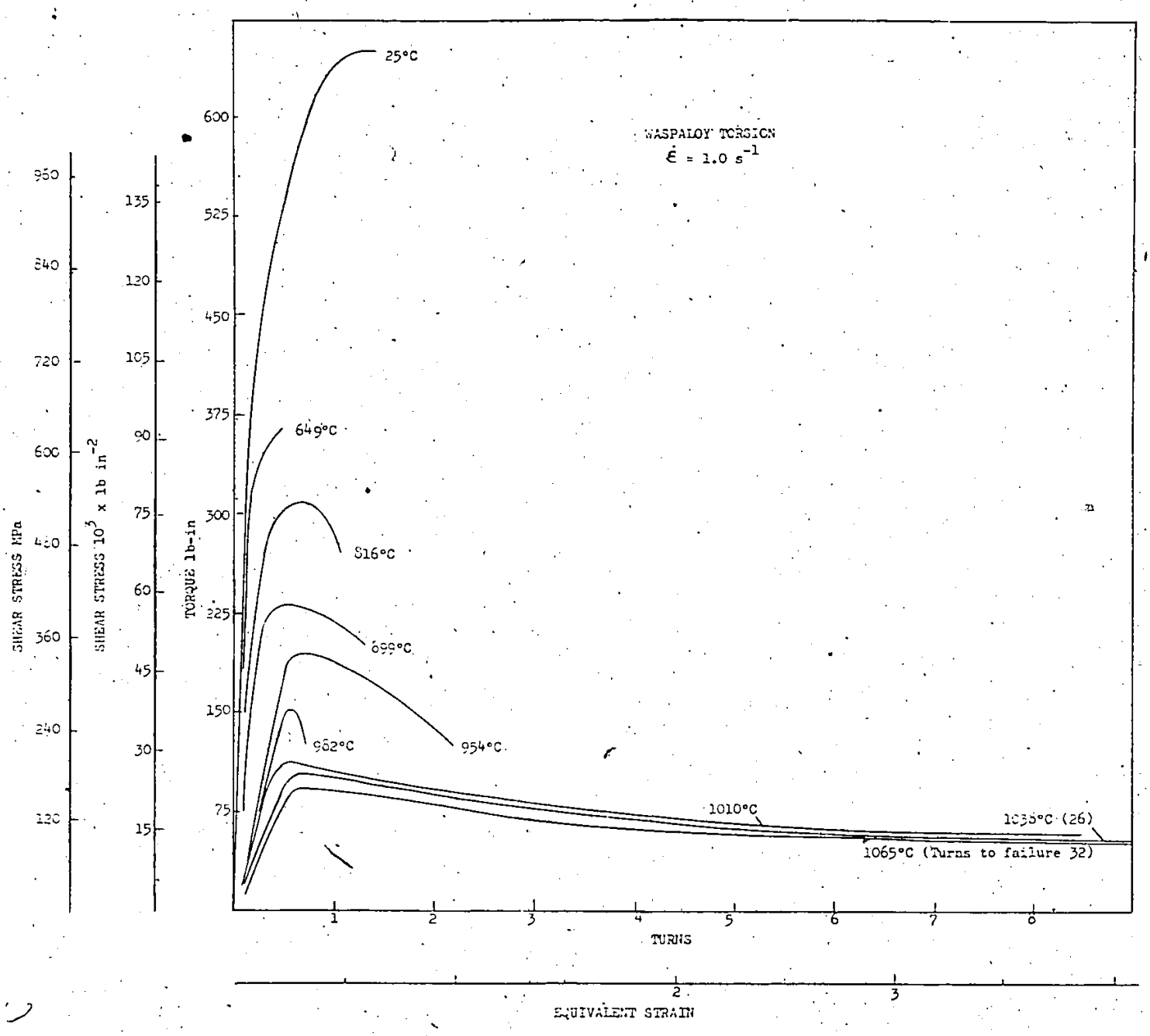
WASPALOY TORSION
$\dot{\epsilon}$ = 1.0 s^{-1}
25°C
649°C
816°C
899°C
954°C
982°C
1010°C
1038°C (26)
1065°C (Turns to failure 32)
TORQUE lb-in
SHEAR STRESS 10^3 x lb in^{-2}
SHEAR STRESS MPa
TURNS
EQUIVALENT STRAIN

Fig. 6-1

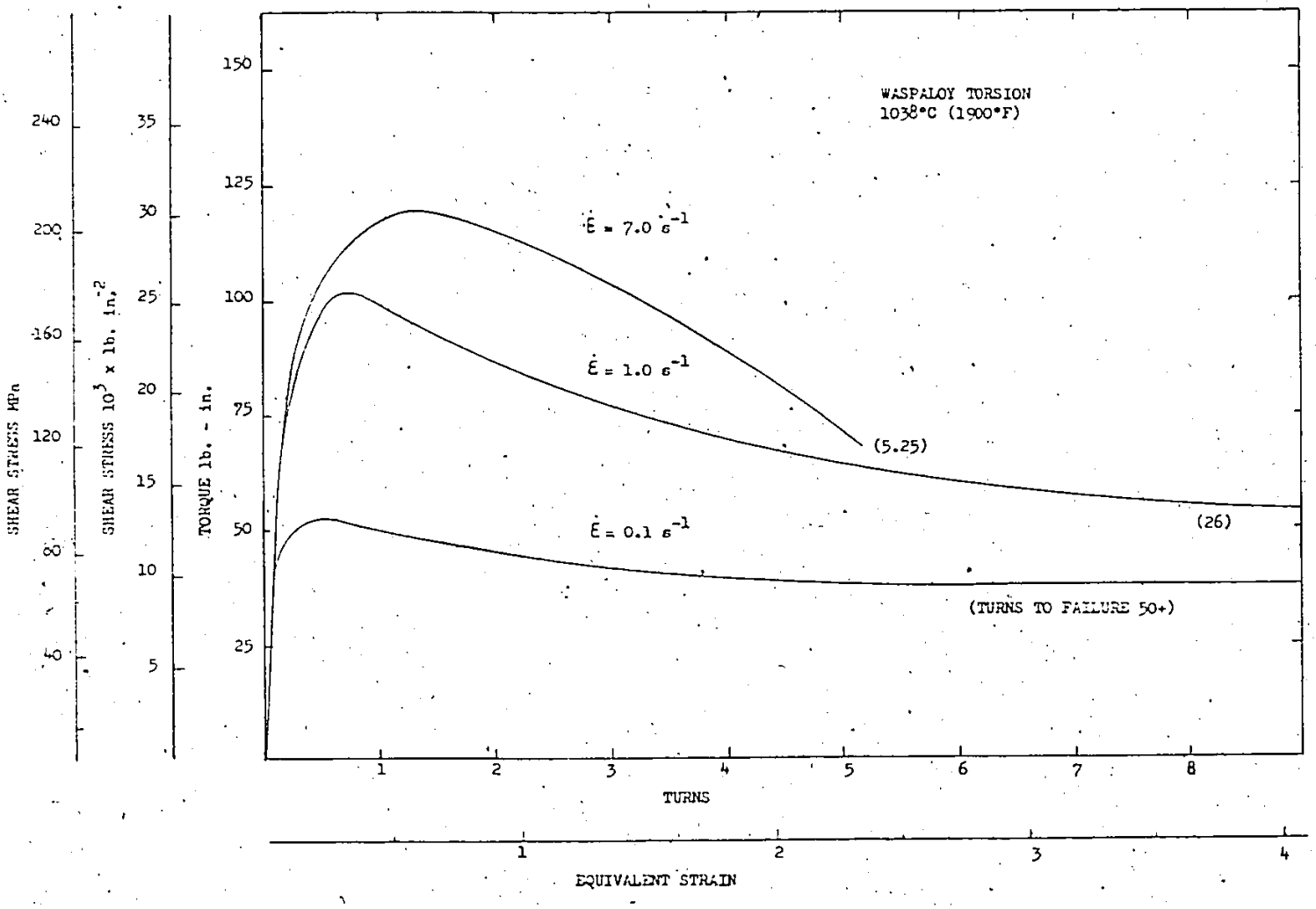
WASPALOY TORSION
1038°C (1900°F)
$\dot{\varepsilon}$ = 7.0 s^{-1}
$\dot{\varepsilon}$ = 1.0 s^{-1}
$\dot{\varepsilon}$ = 0.1 s^{-1}
(5.25)
(26)
(TURNS TO FAILURE 50+)
SHEAR STRESS MPa
SHEAR STRESS 10^3 x lb. in.$^{-2}$
TORQUE lb. - in.
TURNS
EQUIVALENT STRAIN

Fig. 6-2

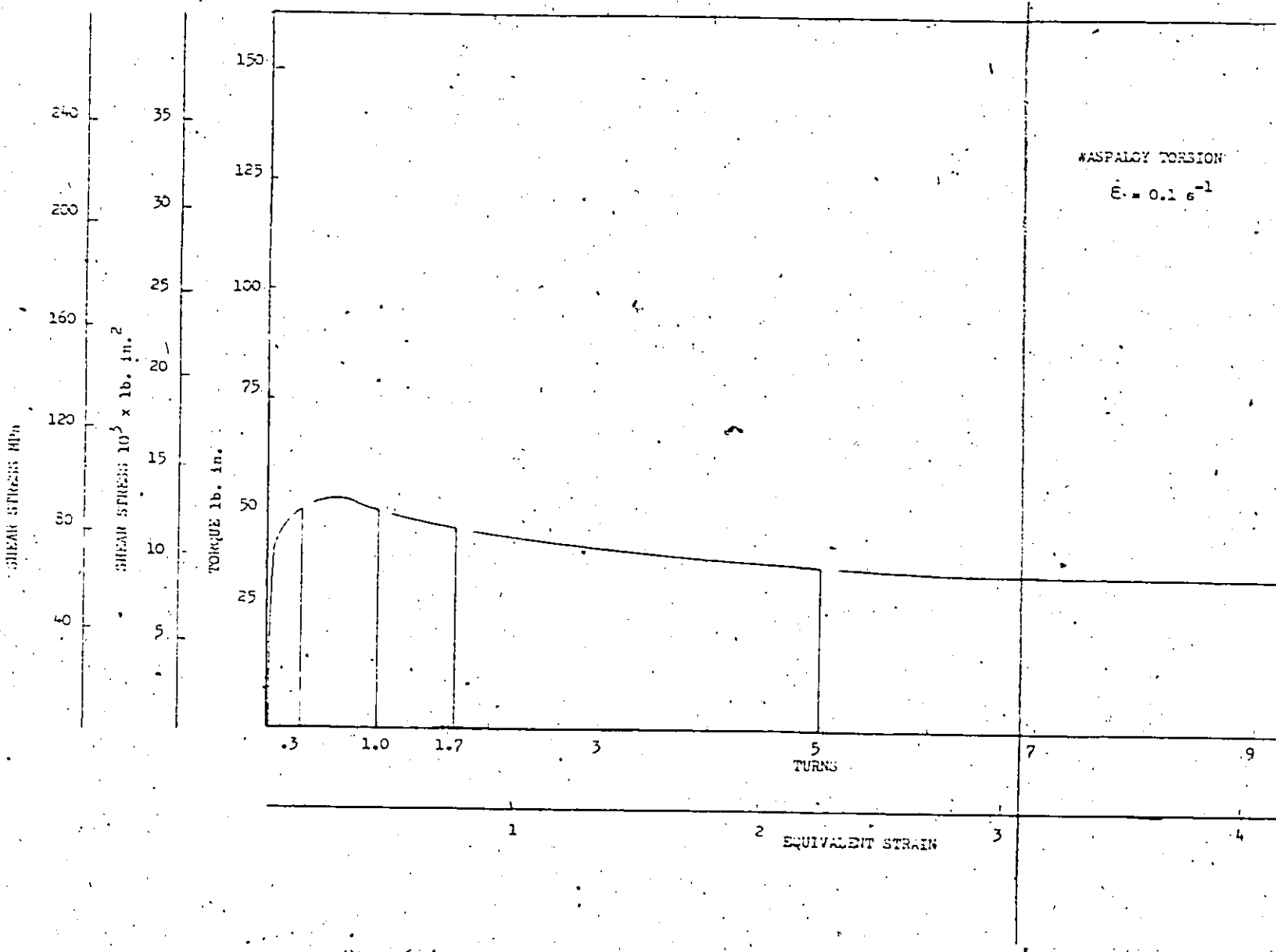
SHEAR STRESS MPa
240
200
160
120
80
40
SHEAR STRESS 10^3 x lb. in.^{2}
35
30
25
20
15
10
5
TORQUE lb. in.
150
125
100
75
50
25
.3
1.0
1.7
3
5
7
9
TURNS
1
2
3
4
EQUIVALENT STRAIN
ASPALOY TORSION
$\dot{\epsilon} = 0.1\ s^{-1}$

Fig. 6-3

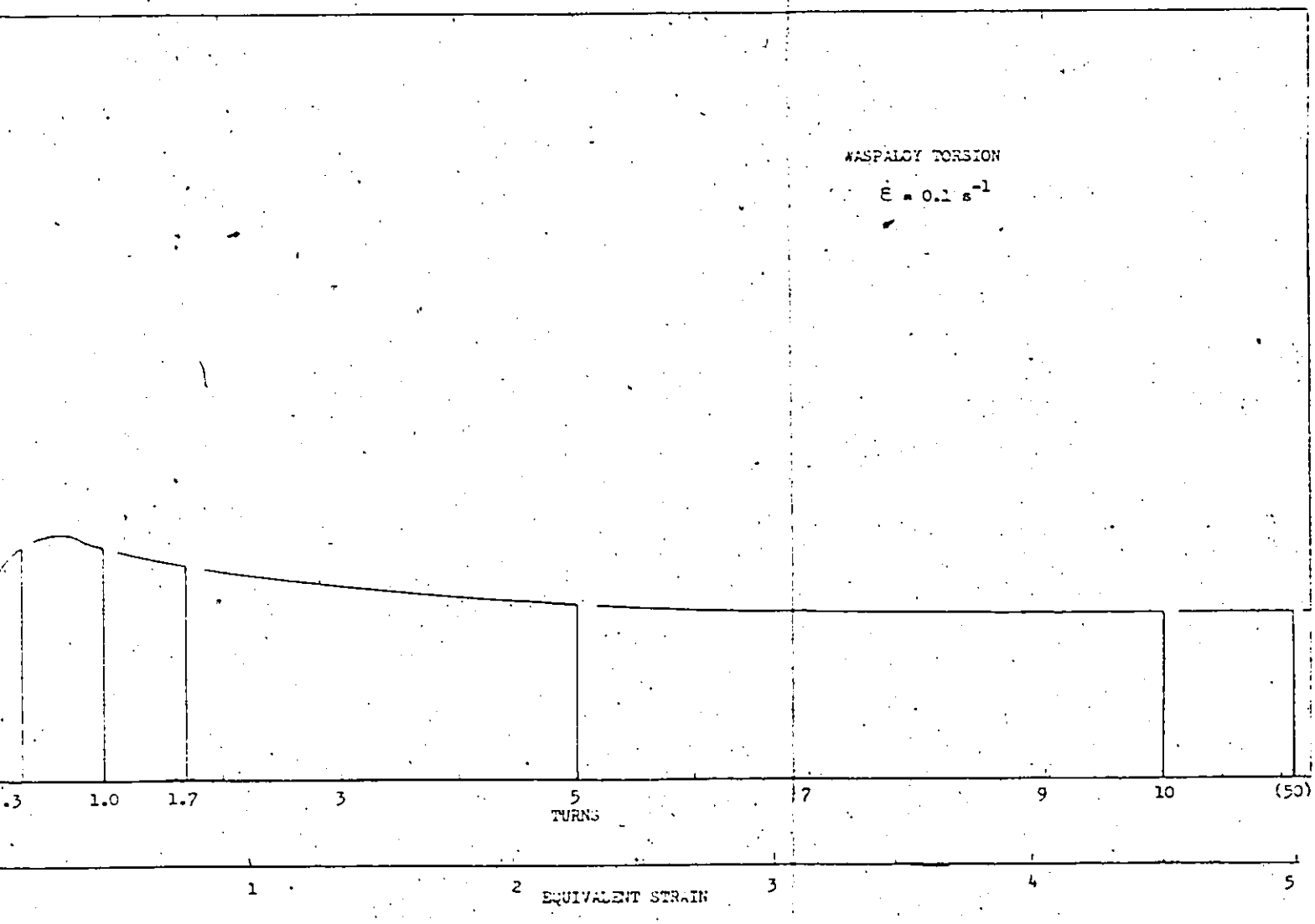
WASPALOY TORSION
$\dot{\bar{\varepsilon}} = 0.1\ s^{-1}$
.3
1.0
1.7
3
5
7
9
10
(50)
TURNS
1
2
3
4
5
EQUIVALENT STRAIN

Fig. 6-3

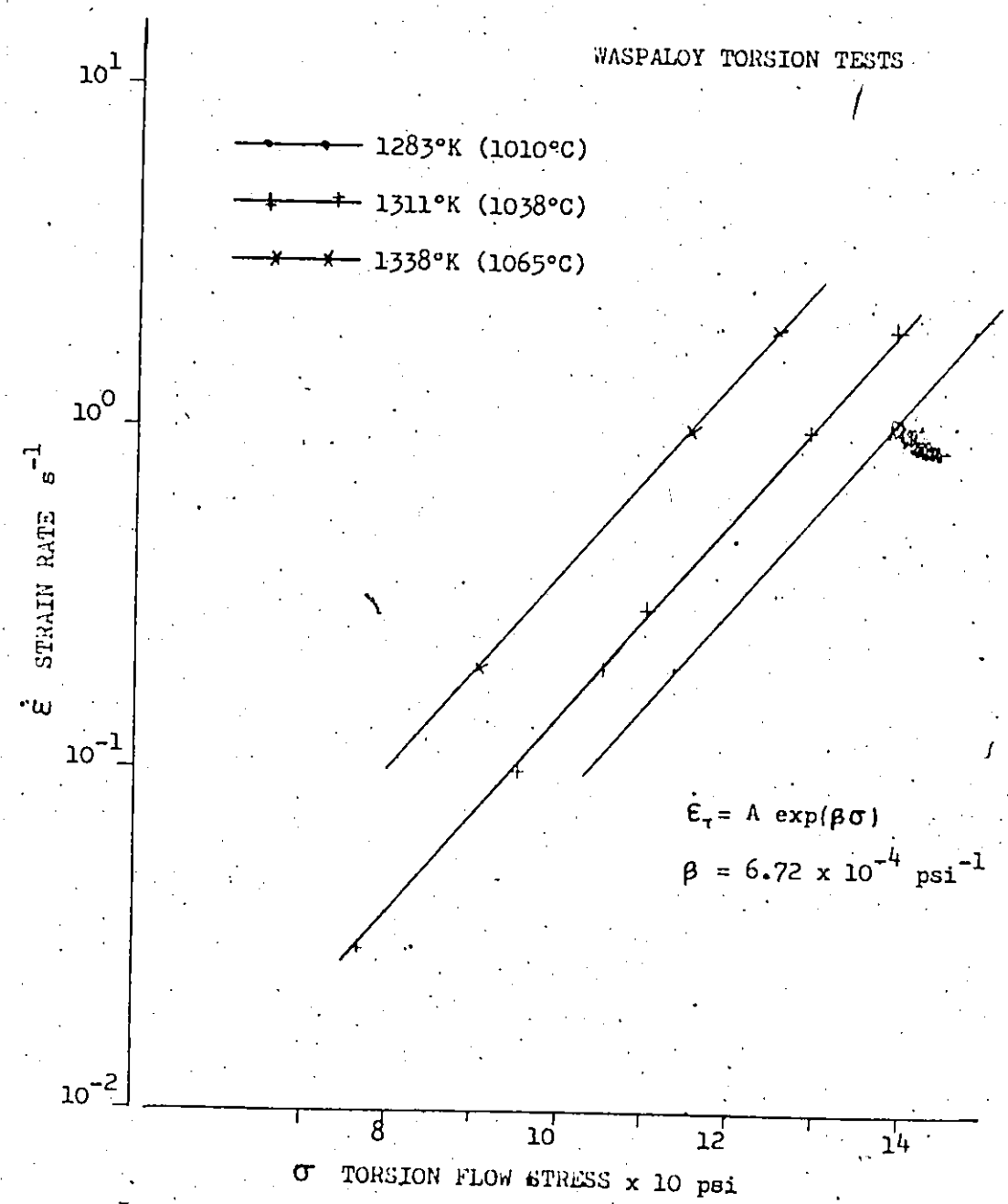

Interdependence of strain rate and stress according to an exponential relationship of the type $\dot{\varepsilon}_\tau = A \exp(\beta\sigma)$

Fig. 7-1

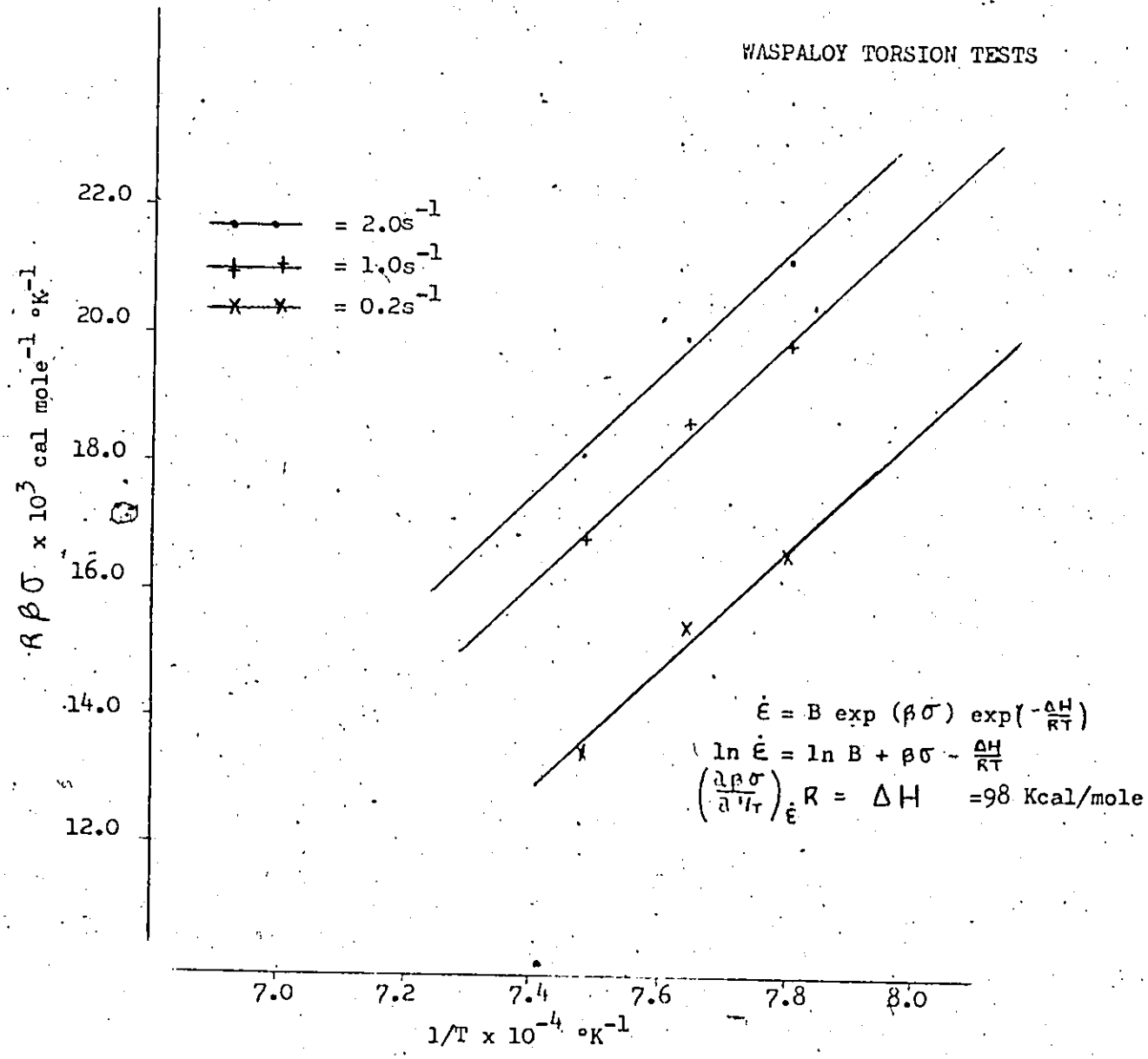

Interdependence of strain rate, flow stress and temperature according to an Arrhenius relationship of the type $\dot{\epsilon} = B \exp(\beta\sigma) \exp(-\frac{\Delta H}{RT})$.

Fig. 7-2

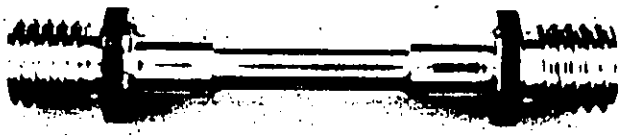

(a) Both ends threaded X1

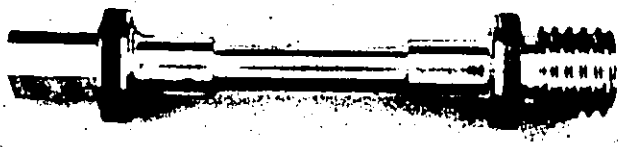

(b) One end rectangular to aid removal X1

(c) Deformed at 1038°C, 7.0 s^{-1}, 5 turns =2.3 X1

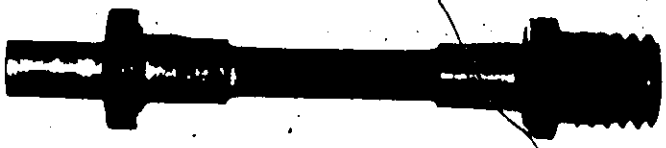

(d) Deformed at 1038°C, 0.1 s^{-1}, 5 turns =2.3 X1

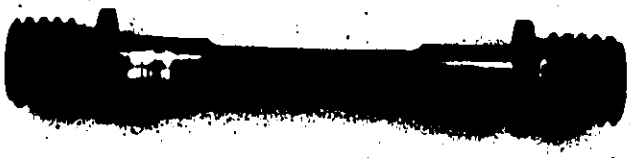

(e) Deformed at 1038°C, 0.1 s^{-1}, 50 turns $\bar{\varepsilon}$=22.5 X1

Fig. 8-1 - Waspaloy, torsion test specimens, (a) undeformed fracture specimen, (b) undeformed interruption strain specimen, (c) (d) (e) deformed at 1038°C at different rates to different strains.

(a) Deformed at 816°C, 1.0 s^{-1}, 1.1 turns, $\bar{\varepsilon}$=0.5 X1

(b) Deformed at 954°C, 1.0 s^{-1}, 2.2 turns, $\bar{\varepsilon}$=1.0 X1

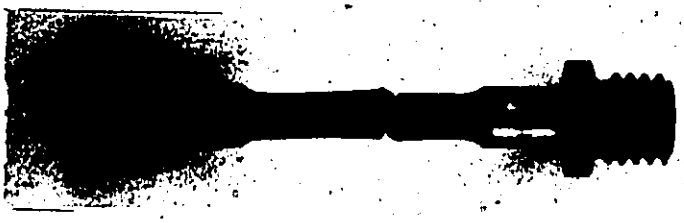

(c) Deformed at 1010°C, 1.0 s^{-1}, 21 turns, $\bar{\varepsilon}$=9.5 X1

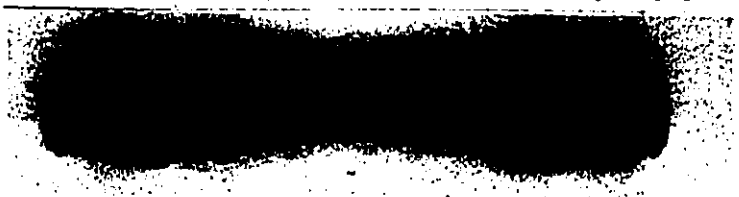

(d) Deformed at 1038°C, 1.0 s^{-1}, 26 turns, $\bar{\varepsilon}$=11.7X1

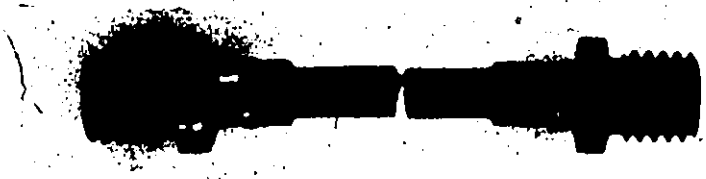

(e) Deformed at 1093°C, 1.0 s^{-1}, 22.2 turns, $\bar{\varepsilon}$=10 X1

Fig. 8.2 - Waspaloy, torsion specimens deformed to fracture at constant strain rate at different temperatures.

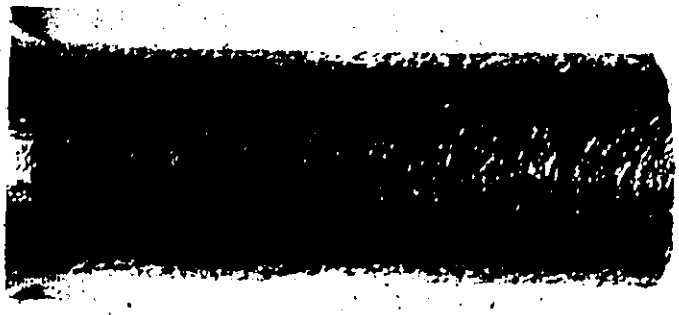

(a) Deformed at 25°C, $1.0s^{-1}$, 1.4 turns, $\bar{\varepsilon}=0.6$ X5

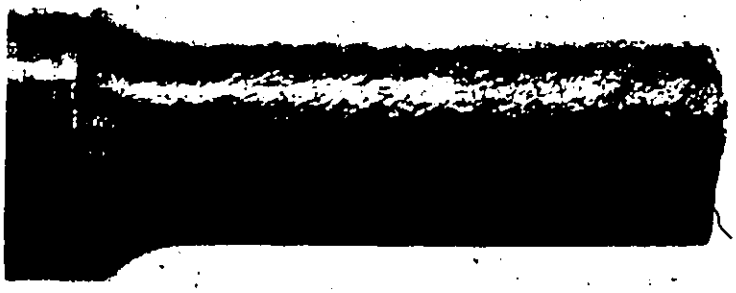

(b) Deformed at 816°C, $1.0s^{-1}$, 1.1 turns, $\bar{\varepsilon}=0.5$ X5

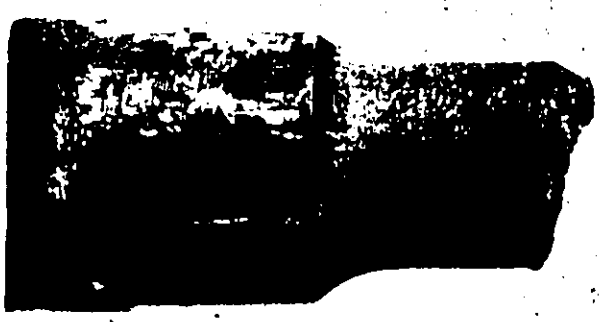

(c) Deformed at 954°C, $1.0s^{-1}$, 2.2 turns, $\bar{\varepsilon}=1.0$ X5

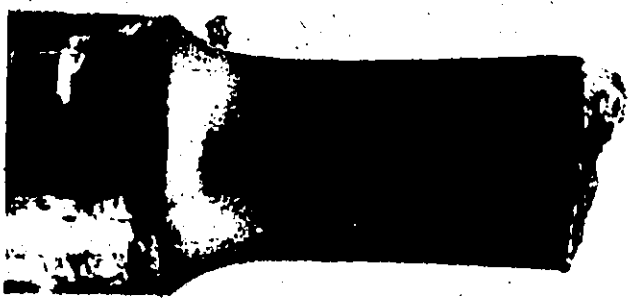

(d) Deformed at 1010°C, $1.0s^{-1}$, 21 turns, $\bar{\varepsilon}=9.5$ X5

Fig. 8-3, Waspaloy torsion specimens deformed to fracture at a constant strain rate of $1.0s^{-1}$ at different temperatures.

(a) Deformed at 1038°C, $1.0s^{-1}$, 26 turns, $\bar{\varepsilon}$=11.8, X5

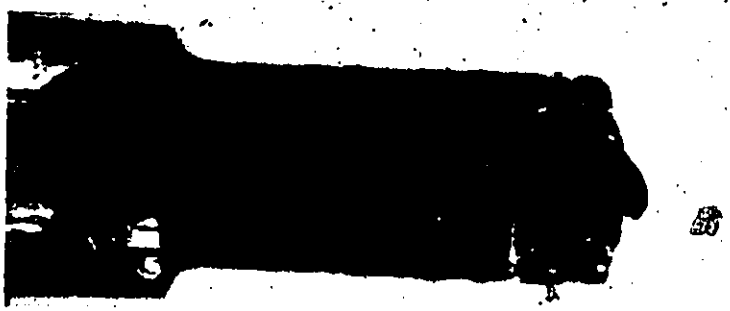

(b) Deformed at 1093°C, $1.0s^{-1}$, 22.2 turns, $\bar{\varepsilon}$=10 X5

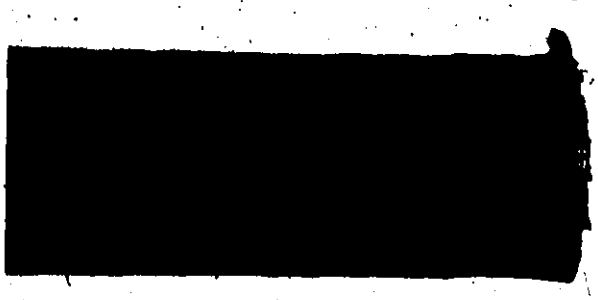

(c) Deformed at 1038°C, $7.0s^{-1}$, 5.3 turns, $\bar{\varepsilon}$=2.4 X5

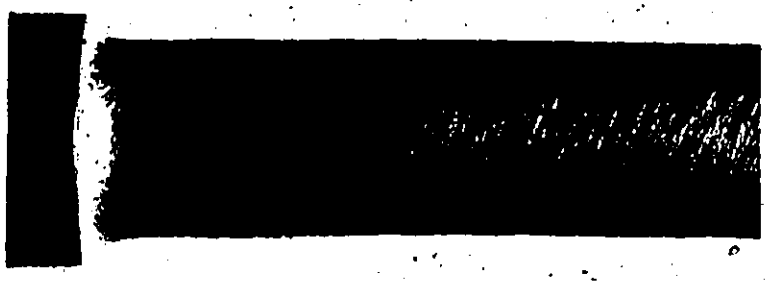

(d) Deformed at 1038°C, $7.0s^{-1}$, interrupted - X5

Fig. 8-4 Waspaloy torsion specimens, (a) and (b) deformed to fracture at constant strain rate of $1.0s^{-1}$, but at different temperatures. (a) and (c) deformed at different strain rates. (d) deformation interrupted at 5 turns, $\bar{\varepsilon}$=2.2.

(a) X110

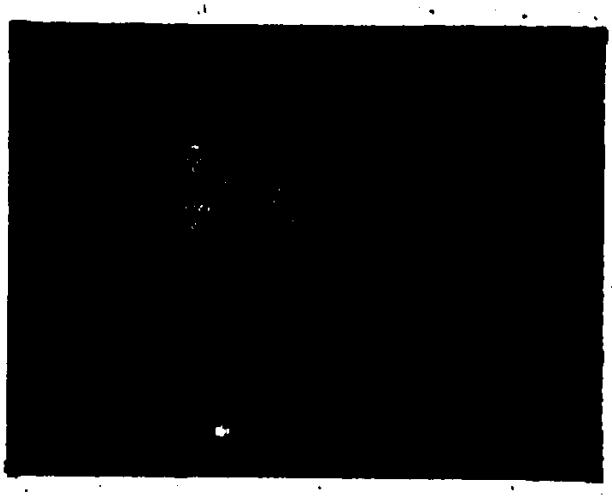

(b) X567

(c) X225

Fig. 9. Waspaloy, torsion, 25°C, 1.0s^{-1}, fractured at 1.3 turns, $\bar{\epsilon}$=0.6.

(a) - Strong deformation markings, at surface in fracture region.

(b) - Cracks in transverse deformation bands inside grains and at ledges on grain boundaries, near surface in fracture region.

(c) - Cracks on grain boundaries, near surface, away from fracture.

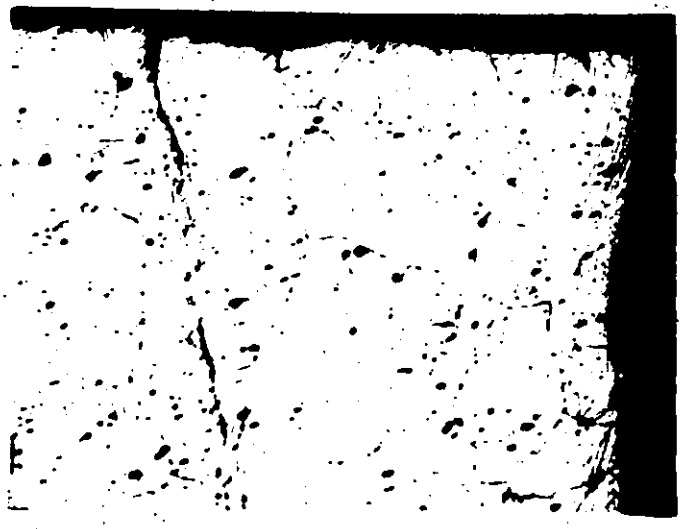

(a) X110

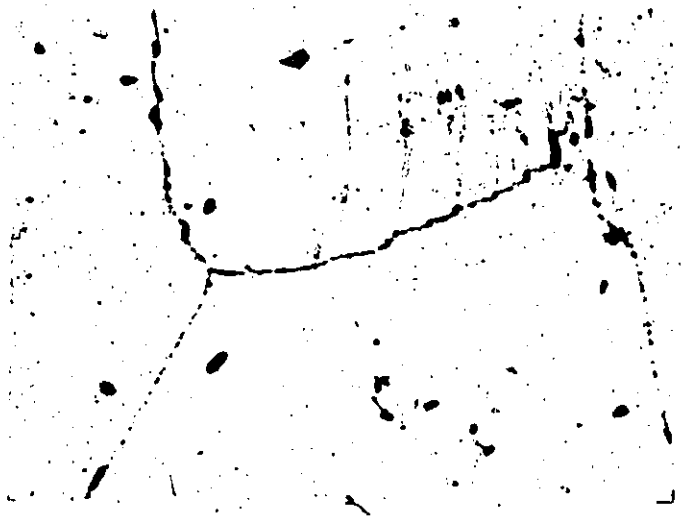

(b) X567

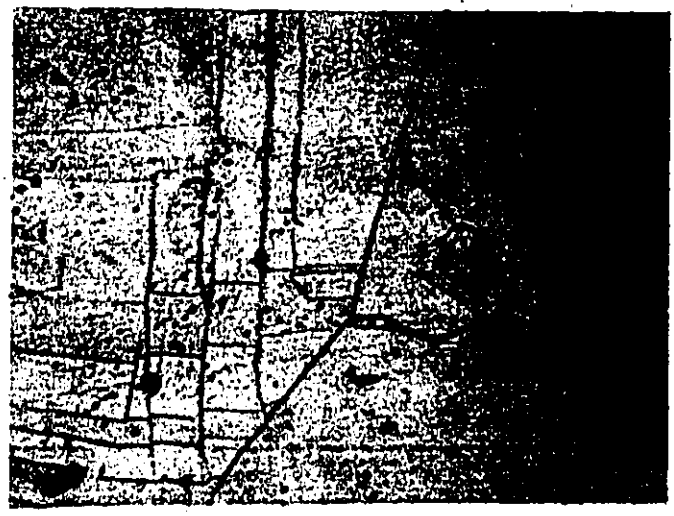

(c) X225

Fig. 10. Waspaloy, torsion, 649°C, 1.0s^{-1}, fractured at 0.5 turns, $\bar{\varepsilon}$=0.2.

(a) - Faint deformation markings and cracks in transverse deformation bands, at and near surface in fracture region.

(b) - Cracks on transverse grain boundaries due to grain boundary sliding and cracks on longitudinal grain boundaries at ledges in deformation bands, near surface in fracture region.

(c) - Cracks in deformation band at ledge on twin boundary near surface away from fracture.

(a) X110

Fig. 11. Waspaloy, torsion, 816°C, 1.0s^{-1}, fractured at 1.1 turns, $\bar{\epsilon}$=0.5.

(a) - Diffuse deformation of grains, cracks in transverse deformation bands, at surface in fracture region.

(b) - Cracks at twin boundaries and on grain boundaries, near surface near fracture.

(c) - Cracks on twin boundaries and on grain boundaries, near surface away from fracture.

(b) X225

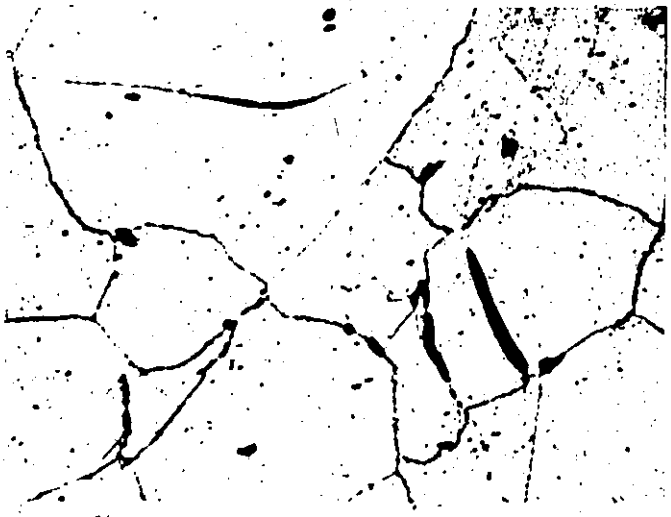

(c) X225

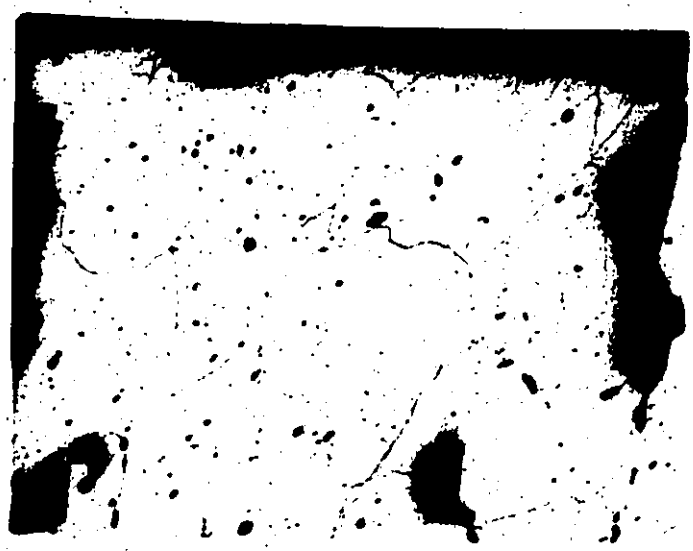

(a) X110

Fig. 12. Waspaloy, torsion, 899°C, 1.0s^{-1}, fractured at 1.4 turns, $\bar{\epsilon}$=0.6.

(a) - Diffuse deformation in grains, cracks in deformation bands and on grain boundaries and twin boundaries in fracture region at surface.

(b) - Diffuse deformation in grains, cracks on grain boundaries and twin boundaries, near surface near fracture region.

(c) - Diffuse deformation in grains, cracks on twin boundaries and grain boundaries, at mid radius away from fracture.

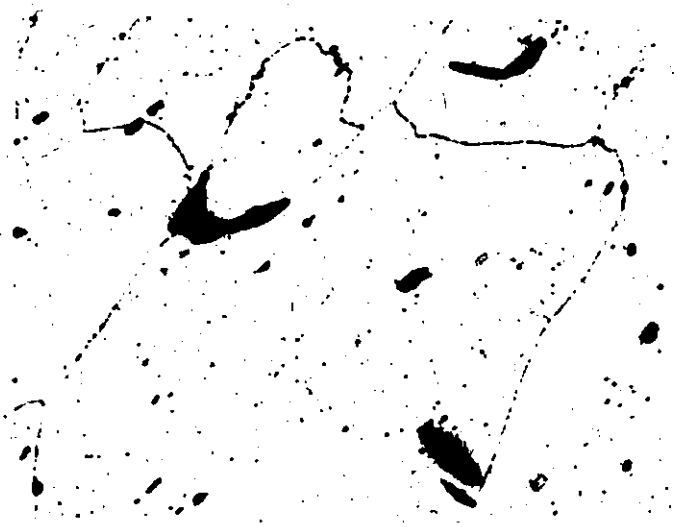

(b) X225

(c) X225

(a) X110

Fig. 13. Waspaloy, torsion, 954°C, 1.0s^{-1}, fractured at 2.2 turns, $\bar{\varepsilon}$=1.0.

(a) - Partial recrystallization and cracks at surface.

(b) - Partial recrystallization and cracks on original grain boundaries and on twin boundaries near centerline in fracture region.

(c) - Partial recrystallization and cracks on twin boundaries, at surface near fracture.

(b) X110

(c) X110

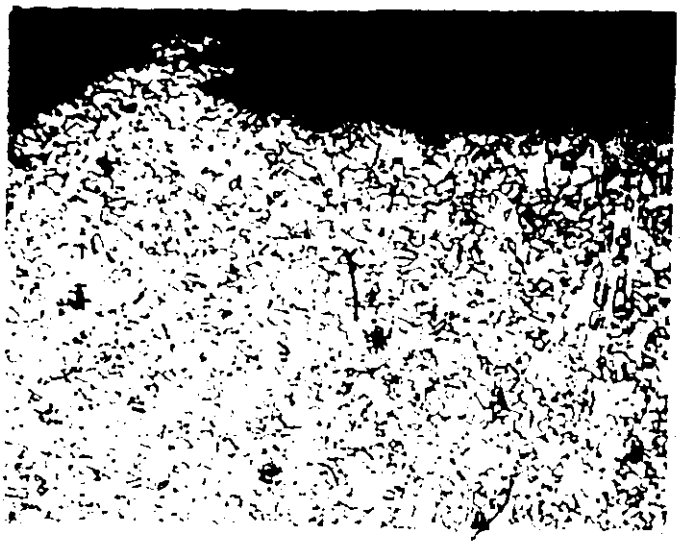

(a) X110

Fig. 14. Waspaloy, torsion, 982°C, $1.0s^{-1}$, fractured at .7 turns, $\bar{\varepsilon}=0.3$.

(a) and (b) - Complete recrystallization, grain boundary pores - linking up to transverse cracks in fracture zone at and near surface respectively.

(c) - Partial recrystallization and cracks at twin boundaries and at grain boundaries, near surface away from fracture zone.

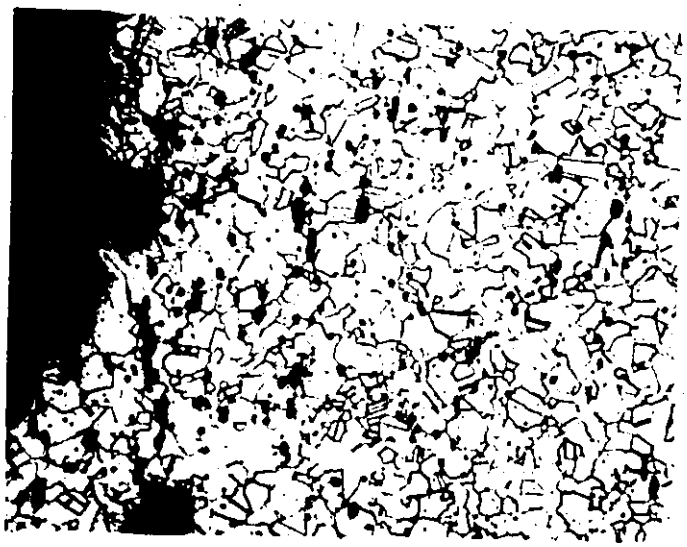

(b) X225

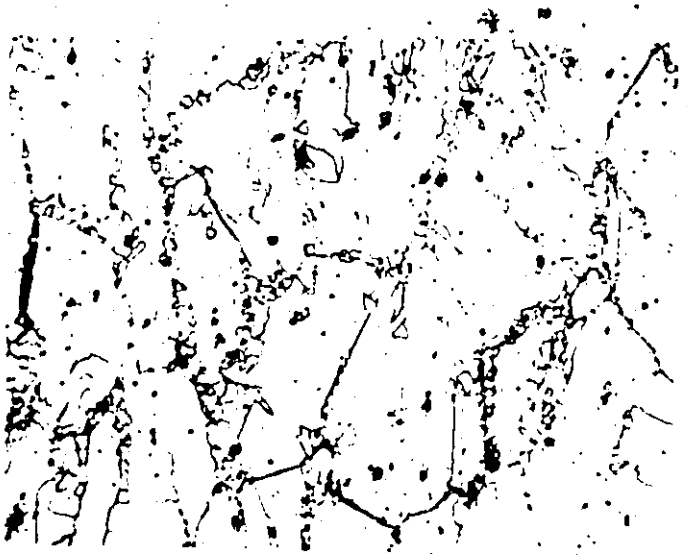

(c) X225

(a) X110

Fig. 15. Waspaloy, torsion, 1010°C, 1.0s^{-1}, fractured at 8.5 turns, $\bar{\varepsilon}$=3.9.

Complete dynamic recrystallization in the whole test section.

(a) and (b) - Pores at boundaries and inside of "new" grains; some pores at carbides, near surface in fracture region.

(c) - Pores and cracks predominantly at carbides; in centerline region away from fracture. Recrystallized grains larger than near surface.

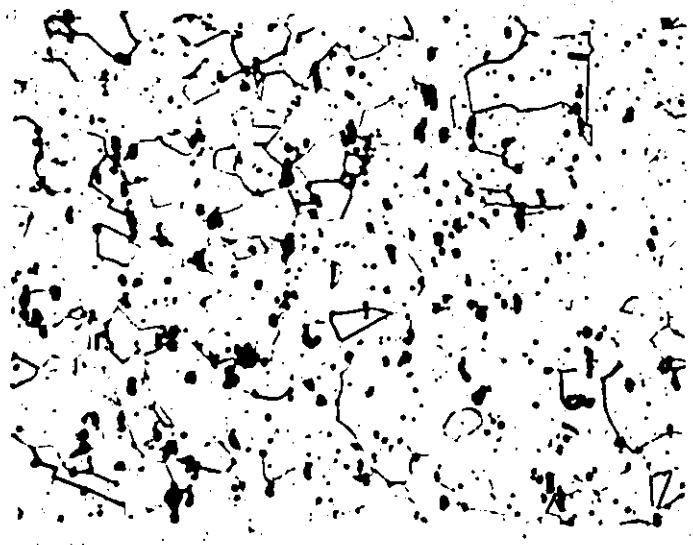

(b) X225

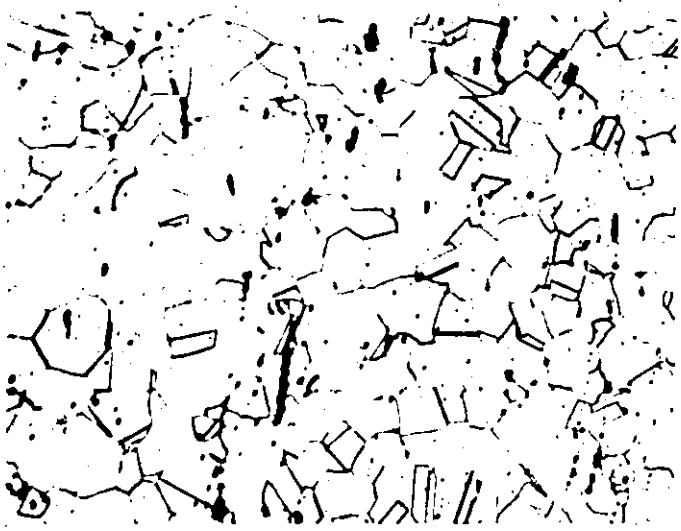

(c) X225

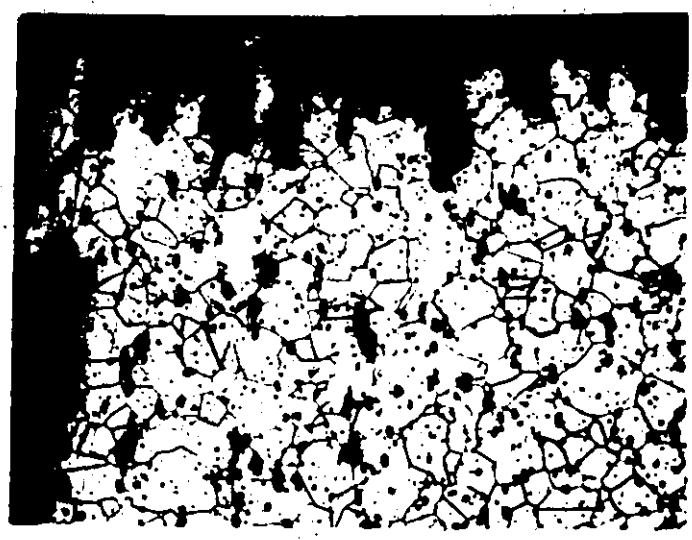

(a) X110

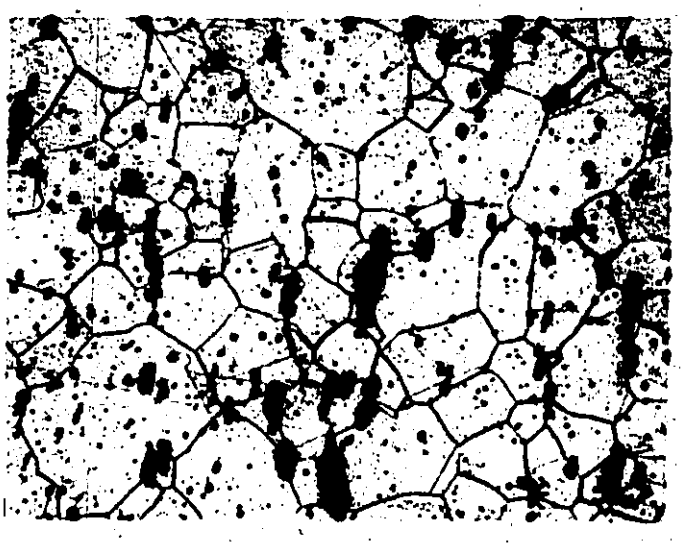

(b) X225

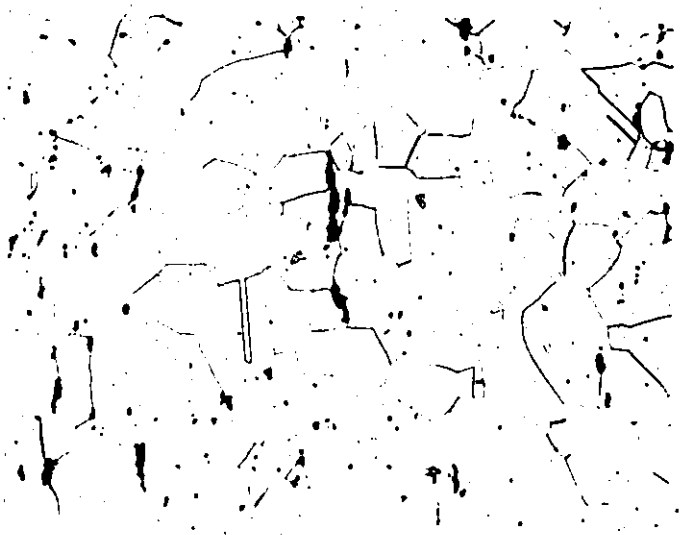

(c) X225

Fig. 16. 'Waspaloy, torsion, 1038°C, 1.0s^{-1}, fractured at 19 turns, $\bar{\varepsilon}$=8.5.

Complete synamic recrystallization in whole test piece.

(a) and (b) - Pores coalescing into microscopic cracks, at and near surface in fracture region.

(c) - Cracks at grain boundaries and at carbides, in centerline region away from fracture.

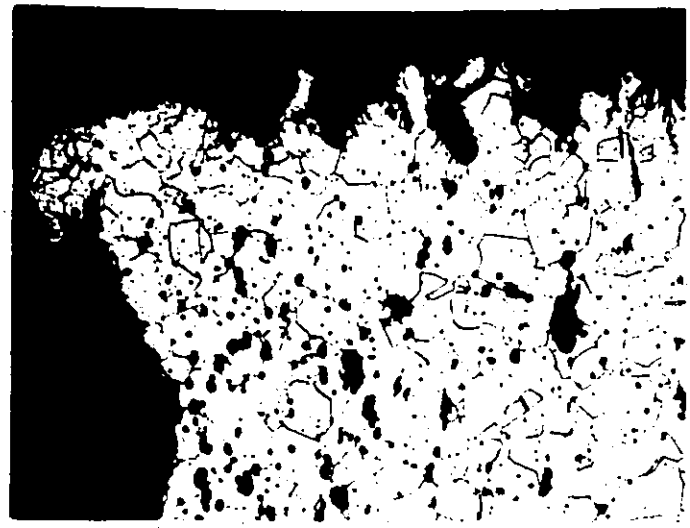

(a) X110

Fig. 17. Waspaloy, torsion, 1065°C, 1.0s^{-1}, fractured at 32 turns, $\bar{\epsilon}$=14.5.

Complete dynamic recrystallization in whole test section. Pores are coalescing into the transverse cracks. Fracture region
(a) at surface
(b) at mid-radius
(c) at centerline

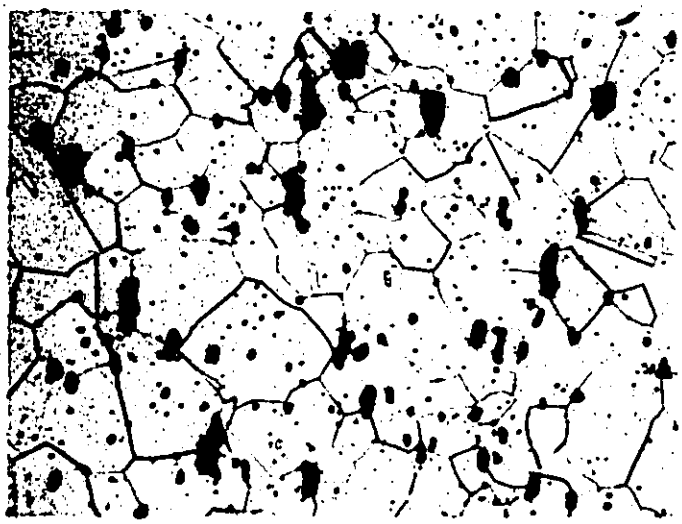

(b) X225

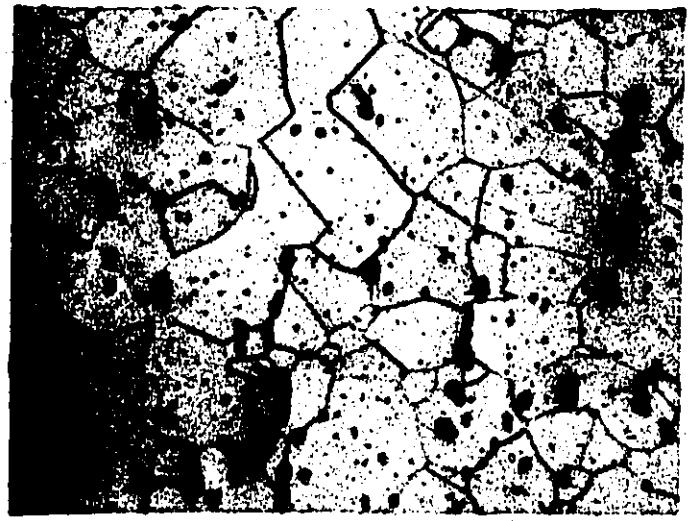

(c) X225

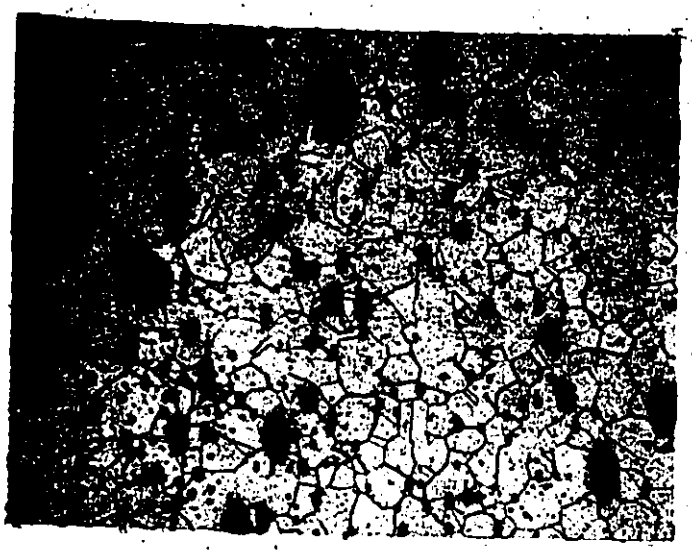

(d) X110

Fig. 17 Continued. Waspaloy, torsion, 1065°C, 1.0s^{-1}, fractured at 32 turns, $\bar{\varepsilon}$=14.3.

Complete dynamic recrystallization in the whole test length. Size and amount of cracks and pores decreases with distance from fracture zone.

Near surface -
(d) - At fracture.

(e) - Midway between fracture and fillet.

(f) - Near fillet at shoulder.

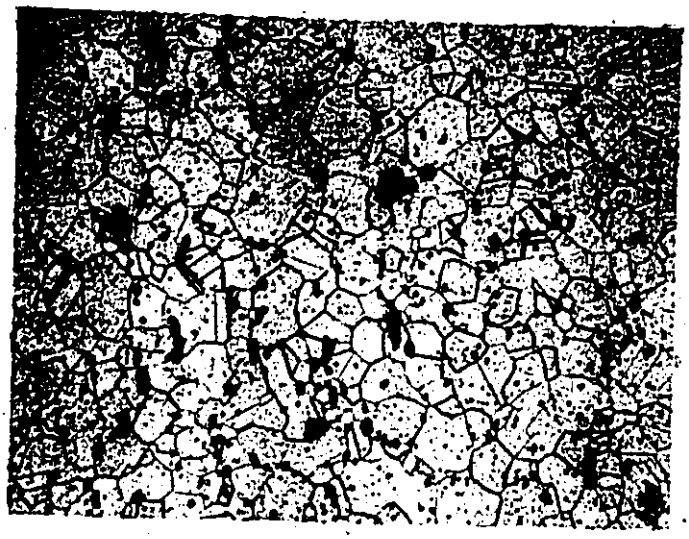

(e) X110

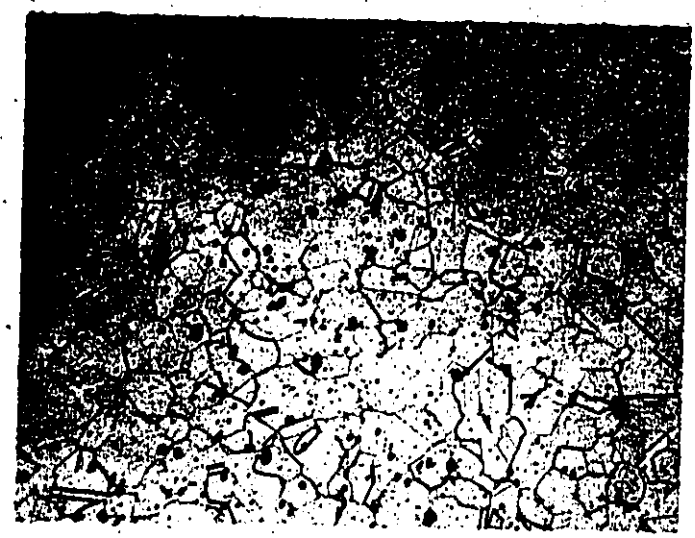

(f) X110

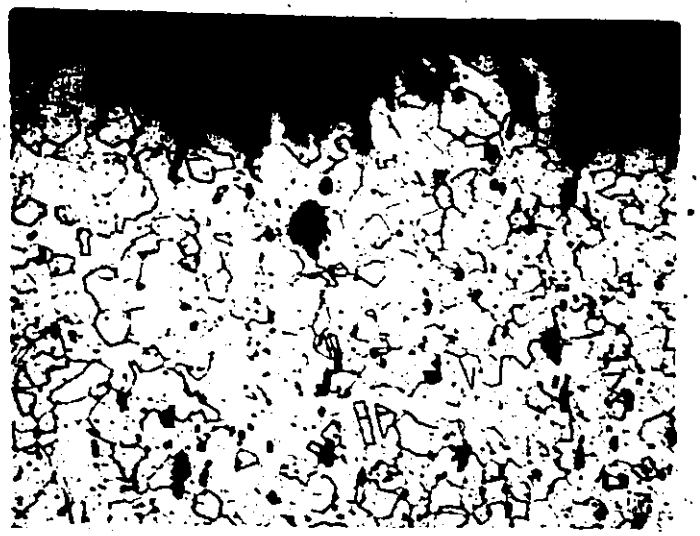

(a) X57

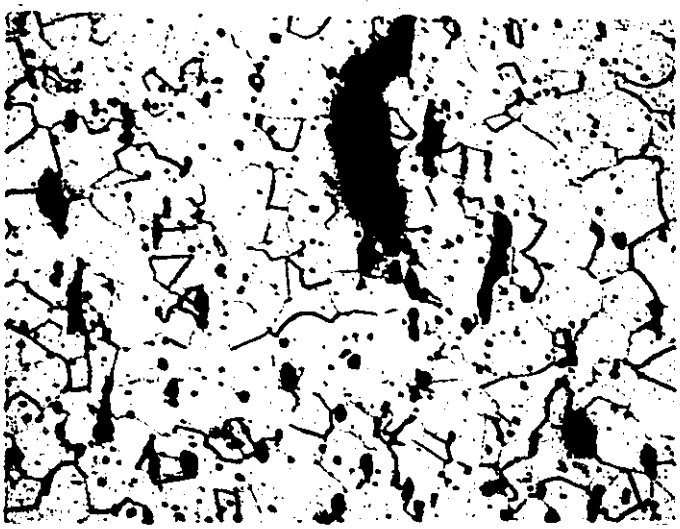

(b) X110

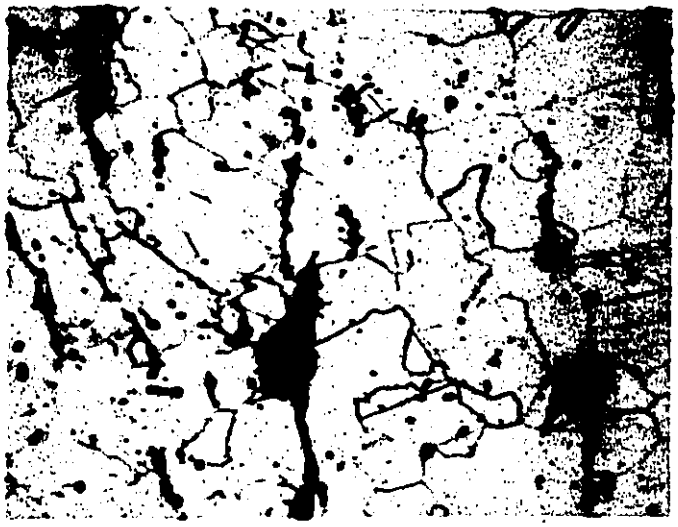

(c) X225

Fig. 18. Waspaloy, torsion, 1093°C, 1.0s^{-1}, fractured at 22.2 turns, $\bar{\epsilon}$=10.

Complete dynamic recrystallization in whole test section; grain size increasing from surface to centerline; pores coalescing into macroscopic cracks in fracture region.

(a) and (b) - At and near surface, at fracture.

(c) - Centerline region at fracture.

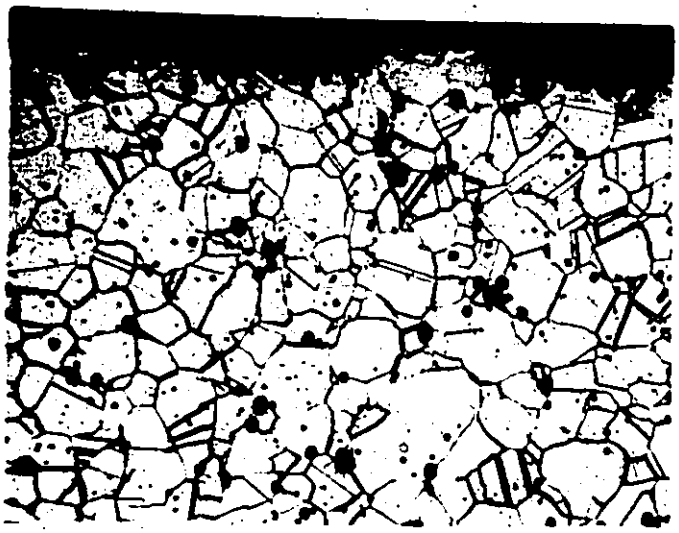

(a) X225

Fig. 19. Waspaloy, torsion, 1038°C, 7.0s^{-1}, twisted to 5 turns, $\bar{\varepsilon}$=2.2, and stopped before fracture.

Complete dynamic recrystallization in surface and mid-radius region; formation of boundary pores: centerline region partly recrystallized with some pores.

(a) - Surface region.

(b) - Mid-radius region.

(c) - Centerline region.

(b) X225

(c) X225

X110

X110

Fig. 20. Waspaloy, torsion, 1038°C, $0.1s^{-1}$, twisted 0.3 turns, $\bar{\epsilon}$ =0.15, then stopped and quenched.

Diffuse deformation in grains, serrated grain boundaries. No recrystallization.

(a) At surface.

(b) Near surface.

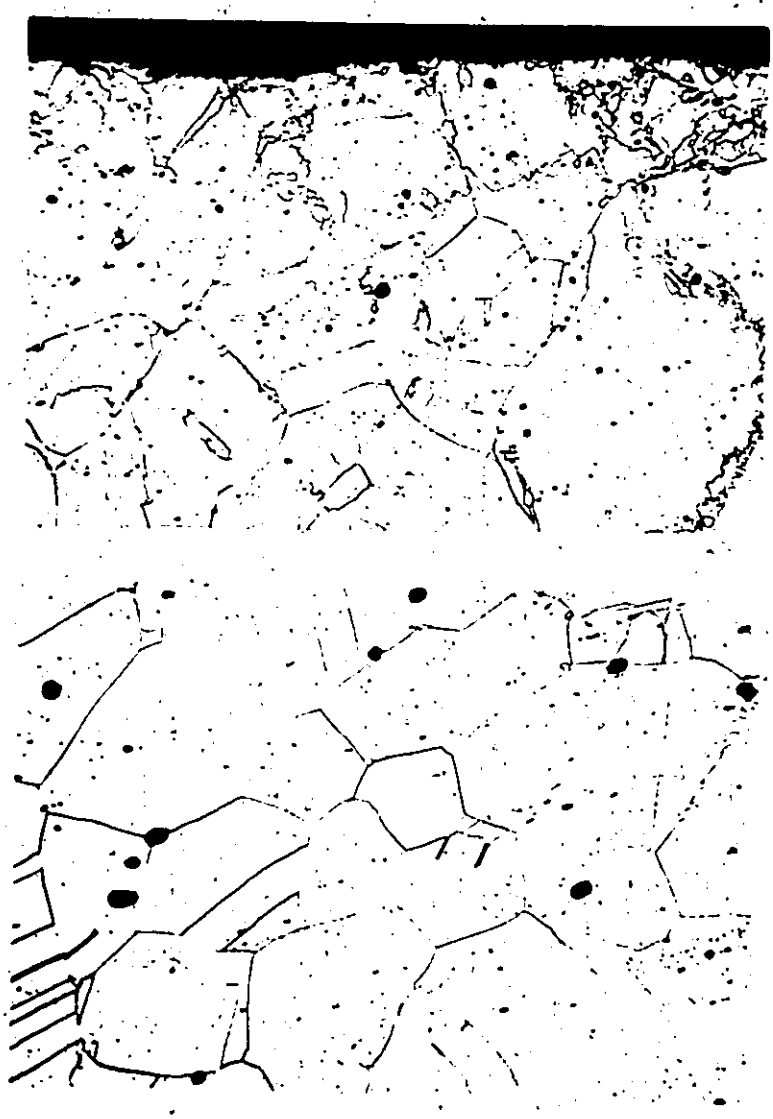

X110

X110

Fig. 21. Waspaloy, torsion, 1038°C, 0.1s^{-1}, twisted to 1 turn, $\bar{\epsilon}$ =.45, then stopped and quenched.

(a) - Initial stage of recrystallization - starting on grain boundaries and twin boundaries at surface.

(b) - Deformed grains, no recrystallization at centerline region.

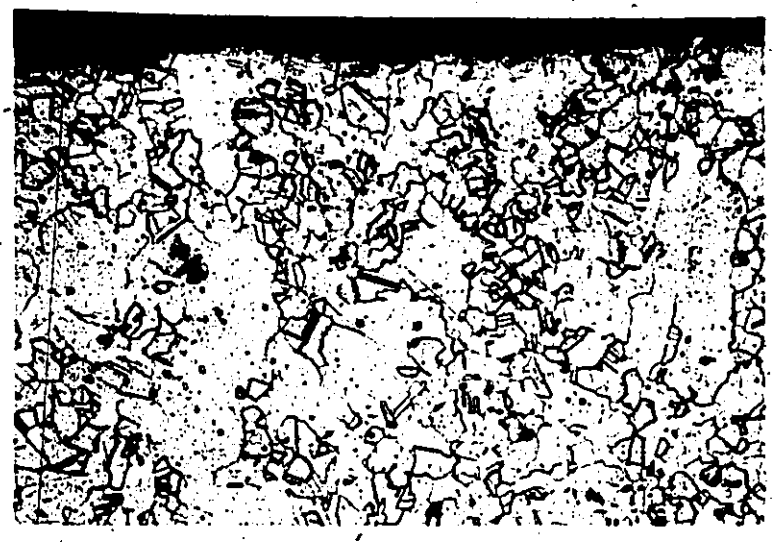

X110

X110

Fig. 22. Waspaloy, torsion, 1038°C, 0.1s^{-1}, twisted to 1.7 turns, $\bar{\varepsilon}$ =0.75, then stopped and quenched.

(a) - Advanced stage of dynamic recrystallization; remainder of original grains still in evidence, at surface.

(b) - Grains deformed, with a few new grains present, centerline region.

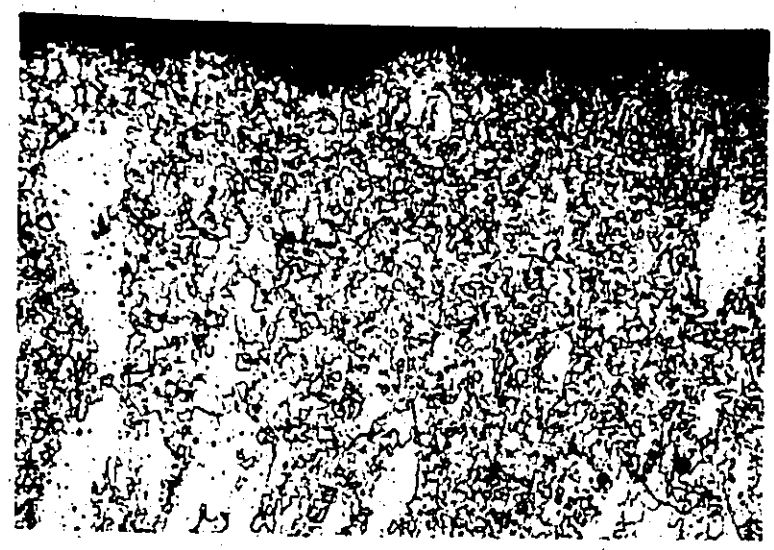

X110

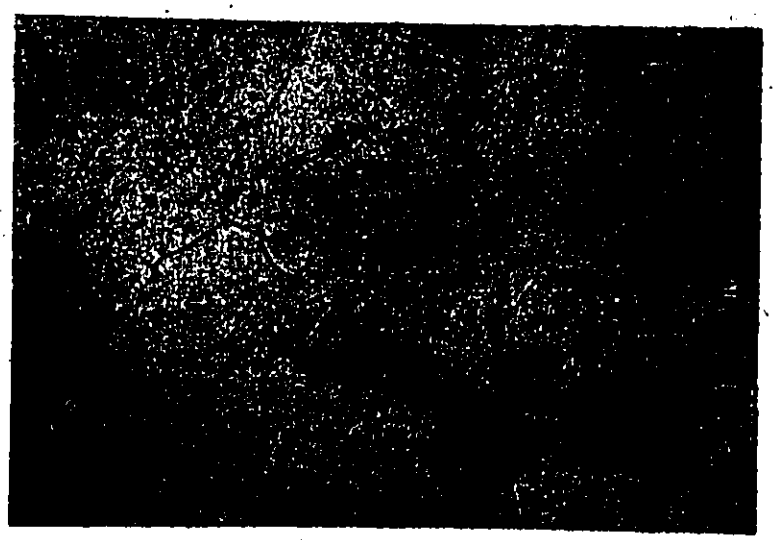

X110

Fig. 23. Waspaloy, torsion, 1038°C, 0.1s^{-1}, twisted to 5 turns, $\bar{\epsilon}$=2.3, then stopped and quenched.

(a) - Almost complete dynamic recrystallization, at surface.

(b) - Partial recrystallization on grain boundaries and twin boundaries of deformed original grains, at centerline.

X110

X110

Fig. 24. Waspaloy, torsion, 1038°C, $0.1s^{-1}$, twisted to 10 turns, $\bar{\varepsilon}$ =4.5, then stopped and quenched.

Deformed into steady state regime of flow curve. Complete dynamic recrystallization.

(a) - Extrusions/intrusions on surface.

(b) - Cracks at carbides at centerline.

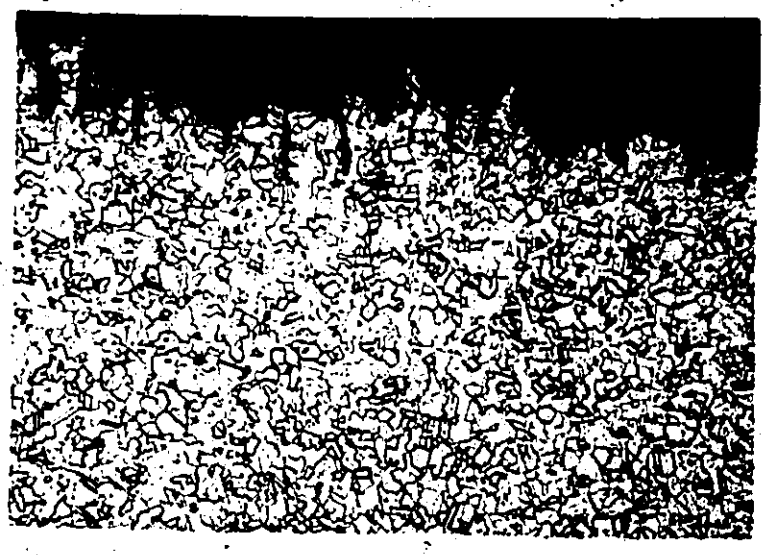

X110

X220

Fig. 25. Waspaloy, torsion, 1038°C, $0.1s^{-1}$, twisted to 50 turns $\bar{\varepsilon}$=22.5, then stopped and quenched.

Deformed well into steady state region, complete dynamic recrystallization.

(a) - Extrusions/intrusions, at surface.

(b) - Centerline region.

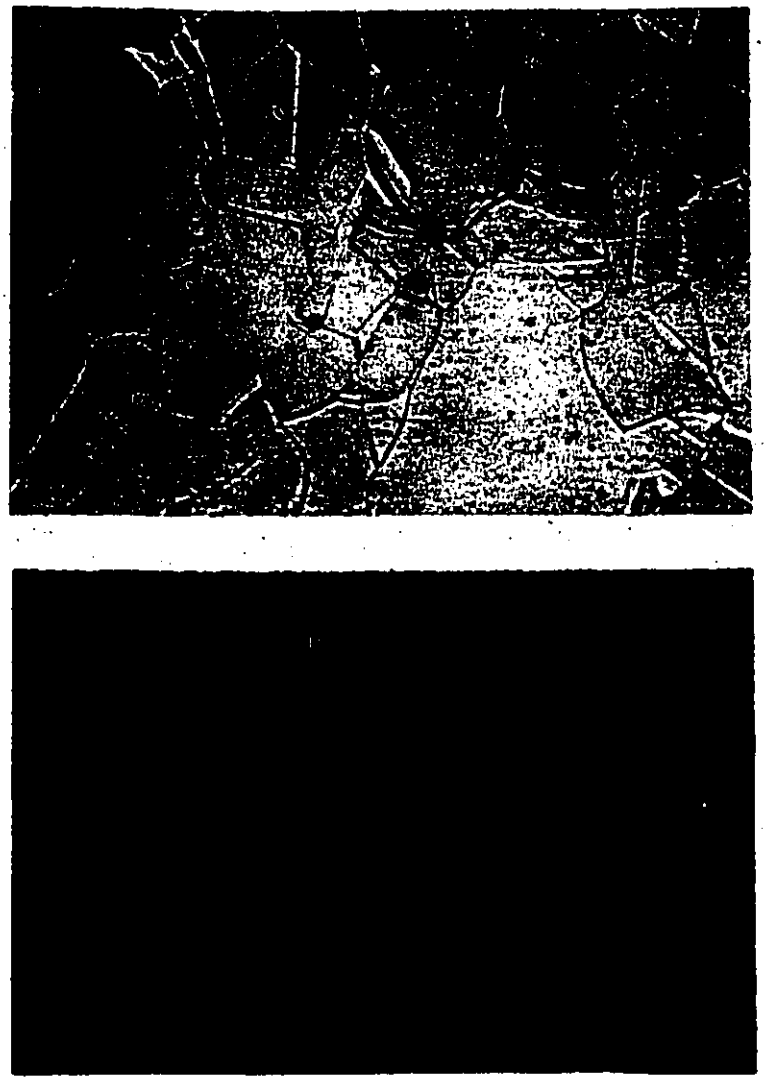

X567

X567

Fig. 26. Waspaloy, torsion, 1038°C, $0.1s^{-1}$, twisted to 1.7 turns, $\bar{\epsilon}$=.75, then stopped and quenched.

First evidence of crack formation.

(a) - Pores on grain boundaries near surface.

(b) - Decohesion at carbides in centerline region.

(a) X567

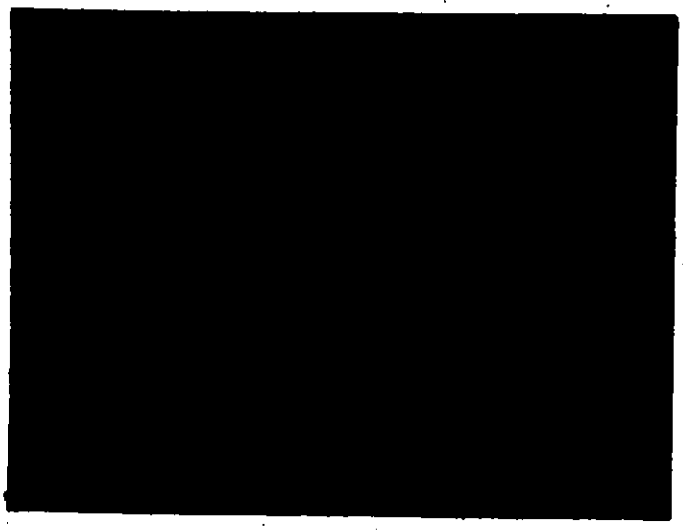

(b) X567

(c) X567

Fig. 27. Waspaloy, torsion, 1038°C, 0.1s^{-1}, twisted to 5 turns, $\bar{\varepsilon}$ =2.3, then stopped and quenched after delay for 7 secs.

(a) - Numerous pores have formed in surface region.

(b) - Some of the pores are at carbides, mid-radius region.

(c) - Few pores present, predominantly at carbides in centerline region.

LIST OF REFERENCES

1. C. Rossard: Metaux, 1960, Vol. 35, 102, 140, 190.
2. H. J. McQueen et al: Can. J. Phys., 1967, Vol. 45, 1225.
3. H. J. McQueen: J. Metals, 1968, Vol. 20, No. 4, 31.
4. J. L. Uvira and J. J. Jonas: Trans. AIME, 1968, Vol. 242, 1619.
5. J. J. Jonas et al: Deformation Under Hot Working Conditions, Iron Steel Inst. Publ. 108.
6. J. J. Jonas, H. J. McQueen and W. A. Wong: Iron Stl. Inst. Publication, 1968, Vol. 108, 49.
7. C. M. Young and O. D. Sherby: AFML-TR-69-294, Stanford Univ., Palo Alto., Calif.
8. J. P. Immarigeon and H. J. McQueen: Can. Met. Qtly., 1969, Vol. 8, No. 1, 25.
9. J. J. Jonas, C. M. Sellars and W. J. McG. Tegart: Met. Rev., 1969, Vol. 14, 1.
10. M. J. Luton and J. J. Jonas: Proc. Int'l Conf. Strength Metals Alloys, 2nd, 1970, Vol. III, 1100.
11. H. J. McQueen and J. E. Hockett: Met. Trans., 1970, Vol. 1, 2997.
12. H. J. McQueen and J. J. Jonas: Metal Forming: Interrelation Between Theory and Practice, 393, Plenum, N. Y.
13. H. J. McQueen and S. Bergerson: Metal Sci. J., 1972, Vol. 6, 25.
14. R. A. P. Djaic and J. J. Jonas: J. Iron Stl. Inst., 1972, Vol. 210, 256.
15. J. P. Sah, G. J. Richardson and C. M. Sellars: J. Aust. Inst. Metals 15, 292.
16. G. Glover and C. M. Sellars: Met. Trans., 1972, Vol. 3, 2271.
17. G. Glover and C. M. Sellars: Met. Trans., 1973, Vol. 4, 765.
18. H. P. Stuwe and B. Ortner, Metal Sci., 1974, Vol. 8, 161.
19. R. D. Doherty: Metal Sci., 1974, Vol. 8, 132.

LIST OF REFERENCES (CONT'D)

20. G. T. Higgins: Metal Sci., 1974, Vol. 8, 143.

21. I. L. Dillamore and H. Katoh: Metal Sci., 1974, Vol. 8, 73.

22. H. J. McQueen and J. J. Jonas: Plastic Deformation Of Materials, R. J. Arsenault, Ed., Academic Press, N. Y. 1974.

23. H. J. McQueen and J. J. Jonas: Materials Forming Conf. Soc. Manufact. Eng., Chicago, 1972.

24. H. J. McQueen and W. J. Mcg. Tegart: Sci. Am., 1975, Vol. 232, No. 4, 116.

25. H. J. McQueen et al: AIME Seminar Hot Deform. Austenite, Ohio, 1975.

26. M. J. Luton and W. J. Mcg. Tegart: Met. Sci. J., 1969, Vol. 3, 142.

27. J. P. Sah, G. J. Richardson and C. M. Sellars: J. Aust. Inst. Metals, 1969, Vol. 14, 292.

28. E. Shapiro, G. E. Dieter and H. A. Kahn: Fracture of Metals During Deformation Processing Under Conditions Of Hot Work, Drexel Inst. Of Tech., Dept. Met. Eng., Philadelphia, Pa., 1969.

29. E. Shapiro and G. E. Dieter: Met. Trans., 1970, Vol. 1, 1711.

30. P. S. Venkatesen and D. N. Beshers: Met. Trans., 1970, Vol. 1, 1780.

31. E. Shapiro and G. E. Dieter: Met. Trans., 1971, Vol. 2, 1385.

32. S. Fulop and H. J. McQueen: 2nd Int'l Conf. Superalloys; Processing, Seven Springs, Pa., 1972.

33. R. E. Bailey: 2nd Int'l Conf. Superalloys; Processing, Seven Springs, Pa., 1972.

34. R. E. Bailey: Metals Eng. Qrtly, May, 1975, 43.

35. D. R. Muzyka: Metals Eng. Qrtly, November, 1971, 12.

36. M. J. Donachie et al: Met. Trans., 1970, Vol. 1, 2623.

37. W. P. Rehrer, R. D. Muzyka and G. B. Heydt: J. Metals, February, 1970, 32.

38. J. M. Oblak, W. A. Owczarski and D. S. Duvall: Met. Trans., 1971, Vol. 2, 1499.

LIST OF REFERENCES (CONT'D)

39. N. Cederblad and N. J. Grant: Met. Trans., 1975, Vol. 6A, 1547.

40. R. K. Hotzler et al: Met. Trans., 1970, Vol. 1, 963.

41. J. M. Oblak and W. A. Owczarski: Met. Trans., 1972, Vol. 3, 617.

42. B. H. Kear, J. M. Oblak and W. A. Owczarski: J. Metals, June 1972, 25.

43. J. J. Jonas and M. J. Luton: 21st Sagamore Conf., 1974, Syracuse Univ. Press.

44. G. E. Dieter: Mechanical Metallurgy, McGraw-Hill, N. Y., 1961.

45. A. Nadai: Theory Of Flow And Fracture Of Solids, McGraw-Hill, New York, 1950.

46. D.S. Fields and W. A. Backhofen: Proc. ASTM, 1957, 1259.

47. S. Fulop, K. C. Cadien, M. J. Luton and H. J. McQueen: A Servo-controlled Hydraulic Hot Torsion Machine, 1974.

48. A. S. Tetelman and A. J. McEvily, Jr.: Fracture Of Structural Materials, Wiley, N. Y., 1967.

OTHER REFERENCES

1. G. P. Sabol and R. Stickler: Phys. Stat. Sol., 1969, Vol. 35, 11.

2. C. T. Sims and W. C. Hegel: The Superalloys, Wiley & Sons New York, 1972.

APPENDIX I

MECHANISMS OF DEFORMATION IN THE HOT WORKING OF NICKEL-BASE SUPERALLOYS

by

S. Fulop* and H.J. McQueen**

* Chief Metallurgical Control Engineer
United Aircraft of Canada
Longueuil, Quebec.
Graduate student
Department of Mechanical Engineering
Sir George Williams University.

** Professor and Chairman
Department of Mechanical Engineering
Sir George Williams University
Montreal, Quebec.

Prepared for presentation at the

Second International Conference on Superalloys: Processing

Seven Springs, Pennsylvania, September 18th, 1972

MECHANISMS OF DEFORMATION IN THE HOT WORKING OF NICKEL-BASE SUPERALLOYS

S. Fulop* and H.J. McQueen**

*Chief Met. Control Eng., United Aircraft of Canada, Longueuil, Quebec.
**Prof., Mechanical Eng., Sir George Williams University, Montreal, Quebec.

A B S T R A C T

The mechanisms of hot deformation have been determined to be dynamic recovery and dynamic recrystallization which control the flow stress developed and the rate of crack propagation. Through their subsequent interaction with static recovery and static recrystallization, which occur whenever the metal remains hot after deformation, they also determine the structure and properties either upon cooling or at entrance to another stage of deformation.

As a preliminary step to understanding the deformation of precipitation hardenable nickel base superalloys; a review is made of the mechanisms observed in the simpler face centered cubic alloys of iron, cobalt and nickel. The hot working behavior of superalloys is reviewed and analyzed in terms of the mechanisms mentioned above.

INTRODUCTION

The nickel-base superalloys are designed for resistance to high temperature creep and oxidation. This resistance is achieved through solid solution with Cr, Fe, Co, Mo and W, precipitation within the grains of intermetallic phases γ', $Ni_3(AlTi)$, and ϵ, Ni_3Nb, and precipitation at the grain boundaries of discrete carbide particles MC, $M_{23}C_6$, M_6C, where M may be Ti, Nb, W, Mo or Cr. Alloys with better creep properties usually have increased quantities of solute and of intermetallic precipitates.

Since these alloys were designed to resist deformation at high temperatures, it is not surprising that they are very difficult to hot work; the ductility is limited and the flow stress is high. Furthermore, any addition in alloying which improves service qualities usually decreases the workability. Increased precipitates require an increased deformation temperature since the alloys are usually worked with the precipitates dissolved. The higher concentration of dissolved alloying elements (40-50% total) gives rise to higher flow stress, higher recrystallization temperature, and lower solidus temperature, thus narrowing the useful temperature range for hot forming. Because of the low thermal conductivity of these highly alloyed materials, contact with cold dies gives rise to severe temperature inhomogeneities (chilling) which diminishes the workability. Furthermore these alloys are subject

during solidification to severe segregation and formation of columnar grains which diminish the ductility during primary reduction. The interdendritic regions of higher than normal concentration have a narrower working range than the homogeneous alloy. These deficiencies can be avoided by use of billets pressed from pre-alloyed powder. In the worked metal, bands of lower alloy concentration have less strengthening carbide and intermetallic precipitates, and larger grain size which comes from lower recrystallization temperature and more rapid grain growth. As a result the product suffers from lowered mechanical properties particularly in the transverse direction.

The objective of hot forming is to produce sound shaped parts of uniform composition and microstructure with grain size suited to subsequent solution, stabilizing and aging treatments. The practical procedures for the working of superalloys have been summarized by Sabroff, Henning and Boulger (1). The purpose of this paper is to reexamine the information about the hot working of superalloys in light of the current theories of deformation and rupture at high temperatures and strain rates. The summary of theory presents only the more important conclusions, omitting most of the supporting detail, because there have been published in the last few years, several reviews of the theories (2-6) and testing techniques (7-8) of hot workability.

The mechanisms of deformation at temperatures above half the melting point of the metal (^{o}K) and at strain rates between 10^{-3} and 2×10^{2} s^{-1} were deduced from microstructural changes and from the inter relationship between the mechanical parameters, which were observed in single phase metals and alloys. In general, the experimental deformations were conducted under conditions of constant and uniform strain rate and temperature. The mechanisms of deformation refer to those occurring during the actual forming and are entitled dynamic. Mechanisms which operate subsequent to the cessation of deformation and before the worked material is cooled down to room temperature are deemed static and are similar to the mechanisms which operate during the annealing of cold worked material. It is important to distinguish these two groups of mechanisms since they can be independently controlled to a certain extent. However, the starting point for the static processes is the microstructure at the end of deformation resulting from the dynamic mechanisms.

HOT WORKING - DYNAMIC RECOVERY

When aluminum is deformed in the hot working range to logarithmic strains between 0.5 and 3.4 and then cooled rapidly, the microstructure consists of the original grains considerably elongated, with a fine substructure and with scalloped boundaries (4 9-12). By means of transmission electron microscopy, the grains are seen to be divided by dislocation sub-boundaries into subgrains with diameters of the order of 2-10 μm (Fig. 1). The substructure resembles aluminum which has been coldworked and softened but not recrystallized by annealing; hence the name dynamic recovery. The subgrain size increases as the temperature of deformation increases or as the strain rate decreases:

$$d^{-1} = -0.6+0.8 \log Z \qquad (12)\ (\text{Eqn. 1})$$

where d = subgrain diameter by ASTM analysis

Z = $\dot{\varepsilon} \exp(+Q/RT)$

= temperature compensated strain rate

$\dot{\varepsilon}$ = strain rate (s^{-1})

Q = activation energy of the mechanism, kcal/mol (kJ/mol)

R = universal gas constant (2 cal/mol ^{o}K) (8.3 J/mol ^{o}K)

T = absolute temperature (^{o}K)

Furthermore as the subgrain diameter increases with decreasing Z, the dislocation density within the subgrains and in the sub-boundaries decreases; the sub-boundaries change from tangles to orderly arrays.

The stress strain curve of aluminum deformed at a constant strain rate and at a constant elevated temperature exhibits a horizontal regime above a strain of approximately 1 which varies inversely with Z. This regime, in which temperature, strain rate and stress do not vary as strain increases, is called steady state deformation and is equivalent to the second stage of creep. During this regime, the subgrain size and misorientation remain constant, thus keeping the dislocation density constant and giving rise to constant flow stress. It thus appears that the rate of annihilation of dislocations (recovery) is high enough to balance the rate of generation of dislocations. The annihilation of the dislocations in the subgrain walls leads to their repeated disruption; subsequently new walls form at an average spacing equal to the subgrain diameter so that the subgrains remain equiaxed, although the grains in which they are embedded become progressively elongated. During the initial hardening regime the dislocations accumulate until equilibrium is attained, this is equivalent to first stage creep. At higher Z, (lower T, higher $\dot{\varepsilon}$) the balance is reached at higher dislocation density since the rate of recovery is lower. The steady-state flow stress depends on the substructure that evolves under the conditions of strain rate and temperature (Fig. 2).

The steady rate flow stress is dependent on the temperature and strain rate of deformation. Of the several mathematical relationships that have been proposed, none have a strict theoretical foundation; a convenient one (Fig. 3) is:

$$f(\sigma) = A\ (\sinh \alpha\sigma)^{n'} = \dot{\varepsilon} \exp(Q/RT) = Z \qquad (11)\ (\text{Eqn. 2})$$

where σ = flow stress in steady state (or at a fixed strain in the hardening regime)

A, α, n', = material constants determined from the test data.

The activation energy, Q, is approximately equal to that for creep or for self diffusion, thus suggesting that the mechanism involves the diffusion of vacancies to climbing dislocations i.e. dynamic recovery. This equation applies not only to hot work but also to creep without any discontinuity (11). The totality of the evidence indicates the mechanisms of creep and hot working of aluminum are identical.

Dynamic recovery appears to be the controlling mechanism of deformation in aluminum. There is, of course, considerable grain boundary sliding but this represents less than one per cent of the strain at hot working rates; its role in rupture will be presented later. Recrystallization during the deformation has never been observed. Moreover the substructure indicates that it is unlikely to occur because dynamic recovery maintains the sub-boundaries at a sufficiently low misorientation that they never become capable of migrating. The substructure seems to be of a scale that prevents the original grain boundaries from bulging into new grains.

After deformation is stopped, the hot worked aluminum can recrystallize if held at the working temperature or if cooled very slowly. If held at the working temperature, the rate of recrystallization is higher, the higher the temperature of working. If a common heat treating temperature is employed after working, the rate of recrystallization is greater the lower the temperature of working since the dislocation density is higher. It is possible, even under industrial conditions, to cool the product sufficiently rapidly to prevent recrystallization and retain the dislocation structure. The flow stress at room temperature varies with the hotwork subgrain diameter:

$$\sigma_y = \sigma_o + 11d^{-1.25} \qquad (13\ 14)(\text{Eqn. } 3)$$

The substructure can be retained in non-heat-treatable alloys to improve the strength and in Al-Cu precipitation hardening alloys to improve the uniformity of precipitate and hence the aged strength. Retention of a subgrain structure improves creep resistance over a limited temperature range (15 16).

During hot working all metals undergo dynamic recovery; however, the mechanism may not be as effective as it is in aluminum so that other mechanisms may come to predominate at larger strains. The body-centered cubic metals, α-Fe, Mo, and W, seem to be very similar to aluminum in their mechanisms and microstructural development. It is other face-centered cubic alloys, such as nickel, copper, and brass, that behave quite differently; the difference becomes greater with decrease in the stacking fault energy, which controls the rate of recovery though its effect on dislocation climb and crossglide. With decreasing stacking fault energy for deformations at the same fraction of the melting temperature ($^{\circ}K$), the subgrains became smaller and the dislocations in the sub-boundaries became more densely packed and more tangled (17). Because of the greater misorientation between the subgrains, a new mechanism, dynamic recrystallization starts during deformation. The strain at which it starts, is less than that for steady-state dynamic recovery and increases as Z increases. Under the usual conditions of temperature and strain rate employed in industrial operations, the critical strain is sufficiently high that dynamic recrystallization does not start in operations such as forging or rolling.

For the metals of low stacking fault energy, because of the very dense substructure, static recrystallization occurs very rapidly when the deformation is stopped, so that it is very difficult to retain the as-worked structure (Fig. 1). It is possible by controlling the strain rate, the temperature of deformation, the strain per pass, the time

between passes, and the cooling rate, to produce a suitable grain size (5 18-20). Such procedures are used in the controlled rolling of plate and in hot-cold work schedules for forging.

HOT WORKING - DYNAMIC RECRYSTALLIZATION

The stress-strain curves for Cu and Ni exhibit a peak which is followed by a decline in flow stress (Fig. 3). The decrease in flow stress is due to the first wave of recrystallization passing through the specimen (4 21 22). If Z is low the flow curve becomes a sinusoidal line in which each peak is the start of a fresh wave of recrystallization and each valley marks the completion of the wave. If Z is high, the strain for completion of a wave of recrystallization overlaps with the strain for nucleation in the material which recrystallized early in the previous stage. The result is a steady state deformation regime in which the flow stress is constant, is lower than the peak stress and is much lower than the steady-state flow stress which would have resulted from dynamic recovery alone. During steady state, the work piece contains a spatially uniform distribution of grains which have different flowstresses dependent on the strains they have undergone since their recrystallization. In the electron microscope specimens which have been quenched extremely rapidly, exhibit small nuclei completely free of dislocations and grains with various densities of substructure (Fig. 1)(23). In the optical microscope, the grains remain equiaxed and similar in size regardless of strain. The grains are large for deformation at lower Z, i.e. lower strain rate and higher temperature.

The dependence of the steady state flow stress on the deformation temperature and strain rate can be expressed by the same equation as that for dynamic recovery (Eqn.2, Fig. 3). However, the activation energy is usually quite different from that for creep or self diffusion and cannot easily be compared with that for static recrystallization because of the variability with even small changes in composition.

After the deformation is halted, recrystallization occurs very rapidly and may occur in two stages which are distinguishable only in certain cases (24 25). The first is meta-dynamic static recrystallization which has no incubation period since it occurs by the continued growth of the dynamic nuclei formed just at the end of deformation. The other is ordinary static recrystallization for which nuclei form in the normal way after the deformation has ceased. The final static recrystallized grain size can be selected by controlling strain rate, temperature, strain per pass, interval between passes and rate of cooling. Industrially there may be little difference in the final product whether the mechanism was solely dynamic recovery or also dynamic recrystallization.

RUPTURE AT HIGH TEMPERATURES AND HIGH STRAIN RATES

The initiation and propagation of wedge-shaped grain boundary cracks has been studied in face centered-cubic alloys with limited ability to recover (35 26-31). The cracks initiated at triple points or ledges as a result of grain boundary sliding which, although only a small fraction of the total strain (32), is still large in comparison with the amount occuring in a creep test. When dynamic recrystallization does not take place, either because the temperature is near the bottom of the hot working range or the strain rate is low, the cracks grow quite rapidly

along stationary boundaries and bring about a low ductility. At higher temperatures, the cracks initiate more frequently but propagate very slowly because the boundaries migrate away from the cracks during dynamic recrystallization. A crack can propagate only when it captures a boundary and then it is only for a short period of time. Under these conditions the ductility is very high and is many times greater than that when dynamic recrystallization is absent. If static recrystallization takes place between stages of deformation then the cracks initiated in the first stage are isolated from the grain boundaries and cannot propagate during the second stage. The most satisfactory criterion for predicting failure on the basis of the deformation conditions appears to be the following equations in which t_r is the time to fracture (Fig. 4)(5 28 29 31):

$$t_r \dot{\varepsilon} = \text{constant} \qquad \text{(Eqn. 4)}$$

and with substitution from Eqn. 2 for $\dot{\varepsilon}$

$$t_r = A' (\sinh \alpha\sigma)^{-n'} \exp (Q/RT) \qquad \text{(Eqn. 5)}$$

The experimentally measured values of n' and Q may be the same as for the experimentally measured strength - strain correlation of Eqn. 2.

The ductility of bcc metals and fcc metals with high stacking fault energy which deform solely by dynamic recovery seems to be higher than those undergoing dynamic recrystallization (3 26 27). It would appear that the formation of a scalloped boundary reduces grain boundary sliding so that cracks do not have an opportunity to grow.

Inclusions or second phase particles which are brittle or much stronger than the matrix and are larger than about 10μm serve as crack initiators and can assist crack propagation by preventing grain boundary migration (3 33-35). The precipitates are most damaging if they are at the grain boundaries in a massive or continuous form. The melting of the alloy at segregated grain boundaries or of a second phase causes the metal to crumble and determines the upper limit of the hot working range.

HOT WORKING OF FACE-CENTERED CUBIC ALLOYS OF TRANSITION METALS

When heat treated for service, the nickel base superalloys constitute a distinct class of alloys because of the corrosion - resistant concentrated-solid-solution matrix and the precipitates of the intermetallic $Ni_3(TiAl)$. However in the condition in which they are usually hot worked ($Ni_3(TiAl)$ in solution) they are a member of a series of face-centered cubic alloys which may be based on iron, cobalt or nickel. Whereas the lower concentration alloys of those three elements exhibit several distinct characteristics, the higher concentration alloys share many similarities because of alloying with each other and with common solutes such as Cr. It is useful to progress from the simpler alloys to the more complex.

Plain Carbon and Low Alloy Steels

The plain carbon and low alloy steels are characterized by a substantial dissolved carbon content which lowers the austenitizing temperature without significantly lowering the temperature for δ formation or for melting. The small quantities of alloying elements which were added for improved hardenability or hardness are in solution. The stress strain curves of Rossard (36), which exhibit a peak followed by steady state or oscillations at lower strain rates, indicate dynamic recrystallization

at high strain. The relations between the flow parameters in steady state follow Eqn. 2 with activation energy varying from 77-110 kcal/mol (322-460 KJ/mol) as carbon content rises. By means of special metallographic techniques, which expose the prior austenite grain boundaries it has been observed that at a strain up to approximately 50% reduction, the mechanism is dynamic recovery which is followed by rapid static recrystallization (18 19 37-39). The strengthening effect of the dynamically recovered substructure has been exploited in the ausforming process. Refinement of the austenite grain size can be achieved by controlling reduction per pass and time between passes in the rolling mill (18-20 40). The ferrite grain size can be made equal to or larger than austenite grain size by controlling the rate of cooling.

The kinetics of static recrystallization have been examined by means of interrupted mechanical tests. Wilbur, Capeletti and Childs (41 42) observed that the rate of recrystallization increased with amount and temperature of deformation so that it was completed in a second at 1015°C (1900°F). Softening by recovery was observed prior to recrystallization. Djaic and Jonas (24 25) have extended the technique to show that meta-dynamic static recrystallization has no incubation period and may be followed by a distinct stage of static recrystallization.

The effect of NbC precipitates which are uniformly distributed and sufficiently fine that they do not initiate cracks have been examined (18-20). The particles raise the flow stress presumably by limiting recovery and stabilizing the substructure as has been observed in creep (42 43). By preventing grain boundary migration, the particles decrease the rate of static recrystallization by two orders of magnitude compared to plain carbon steels. This makes possible the production of an ultra-fine austenite grain size which transforms to stronger, tougher ferritic-pearlitic structures. If the austenite is allowed to transform to ferrite before it recrystallizes, the finest ferrite grain size is approximately equal to the shortest dimension of the austenite grains; thus, the refinement is dependent on the reduction and the initial austenite grain size. It would appear that these precipitates prevent dynamic recrystallization at high strains.

As the concentration of dissolved alloying elements increases, the hot strength increases by 25 to 50% (1 45), and the ductility diminishes by as much as 50% (Ni and Mn in small quantities increase ductility). The ductility usually increases with increased rate of deformation but this may only be the result of adiabatic heating. Inclusions play a prominent role in initiating fracture. Robbins, Shepard and Sherby (33 34) have shown that, when the steel cools into the α/γ two-phase region, the formation of α lowers the ductility substantially (35).

Cobalt

Hot torsion stress-strain curves of face centered cubic cobalt by Jacquerie and Habraken (46) have the peak and steady state regime characteristic of dynamic recrystallization.

Nickel

In torsion tests of nickel (21 29 47-49), the characteristic stress-strain curve exhibits a peak followed either by a steady state regime or at low strain rates by oscillations. Luton and Sellars (47) correlated the strength, strain rate and temperature by Eqn. 2. The activation energy for pure nickel was found to be 56 kcal/mol (234 KJ/mol) which is considerably lower than that for self diffusion. These results in association with the following microstructural evidence are indicative of dynamic recrystallization. Specimens rapidly cooled from the steady state region appear recrystallized but contain a dislocation substructure. In some cases, nucleation occurred by grain boundary bulging. Specimens deformed less than the peak strain

exhibit a subgrain structure (17) and an incubation time for the start of recrystallization but there is none for specimens deformed into steady state deformation.

Sah, Richardson and Sellars (40) measured the incubation time and critical strain for dynamic recrystallization as a function of strain rate at 880°C(1616°F). As the rate of strain increased, recrystallization started at shorter times but after greater critical strains. From the observed rate of recrystallization, the rate of strain hardening (stress-strain curve before the peak) and the critical strain, it was possible to make a calculation of the shape of the stress strain curve after the peak which agreed with the experimental data. At high strain rates and high temperatures the time to reach the critical strain at any point is less than the time for completion of recrystallization in the region, some points will begin to recrystallize a second time before the entire region has recrystallized, thus the dynamic recrystallization occurs continually. On the other hand, at low strain rates, the time to reach the critical strain at any point is much greater than the time for recrystallization of the whole region with the result that the dynamic recrystallization is periodic and the flow stress oscillates.

The time to fracture was related by Luton and Tegart (31) to the conditions of deformation by Eqn. 5. In Fig. 5, grain boundary cracks were halted as the boundaries were removed by dynamic recrystallization. The isolated cracks often became amoeba like voids. Fracture occurred by the linking up of the voids. Shapiro and Dieter (29) divide the rupture behaviour of nickel into three temperature ranges; in all cases the cracking starts at the peak stress. In the low temperature range the metal strain hardens up to a fairly high strain and fractures at the peak stress by transgranular shear. In the intermediate range in which there is no dynamic recrystallization, wedge-shaped cracks form at grain boundaries and extend rapidly to give very low ductility with little extension after the peak. In the high temperature range in which dynamic recrystallization takes place, the grain boundaries migrate away from any cracks that form thus preventing them from propagating. After the peak stress, the flow stress declines to the steady state level and high strains are possible before ultimate fracture. At low strain rates where the recrystallization is periodic, the boundaries remain stationary for longer periods so that a much more extensive crack network forms and there is lower ductility than at high strain rates. The temperature for transition from intermediate to high ranges and the strain for the maximum stress increase as the strain rate is raised.

Luton, Sellars and Tegart (31 47) also studied the behaviour of Ni-Fe alloys up to 20% Fe and found it to be similar to that of pure nickel. The stress at the peak strain and in steady state increased as the Fe content increased; however, this effect diminished as the temperature increased to $0.9T_m$. For strains less than the peak, the incubation time for static recrystallization increases with iron content. The interdependence of the flow parameters obeyed Eqn. 2 with activation energies of 71 kcal/mol(298 kJ/mol) for 5% Fe, 81(339) for 10% Fe, and 94(393) for 20% Fe. Between 762°C (1403°F) and 1279°C (2334°F), the dynamically recrystallized grain size during steady state decreases as the flow stress increases according to the equation.

$$\sigma_{ss} = K \cdot d_G^{-3/4} \qquad \text{(Eqn. 6)}$$

where K decreases from 1.45 for pure Ni to 0.82 for 20% Fe. This indicates that for a given flow stress the grain size of the alloys is lower as the Fe increases because the dissolved Fe decreases the rate of boundary migration. The flow stress must be controlled by the dislocation substructure rather than by the grain size.

Alloys of Fe-25%Ni have been studied by White and Rossard (30). Metallographic examination confirmed dynamic recrystallization was taking place during the steady state

deformation which followed the peak in the stress-strain curve. Crack propagation was inhibited and ductility augmented whenever dynamic recrystallization took place or whenever static recrystallization occurred during the intervals between passes.

Austenitic Stainless Steels

The results presented refer to the most widely studied steel of this type which is Fe-18%Cr-8%Ni; only significant differences for other alloys will be mentioned. Rossard (36) determined the stress strain curves over a range of temperature and strain rate showing that the curves had the characteristic shape for dynamic recrystallization (Fig. 2)(50 51). The flow parameters could be correlated by Eqn. 2 (Q=97 kcal/mol)(405 kJ/mol) and the flow stresses were approximately twice those of carbon steels as a result of the high rate of strain hardening (1 36). In general, the hot strength was greater and the ductility lower when the starting grain size was larger and the amount of Cr, Mo or W increased (1 45 52). After deformation in the steady state regime, the grain size was finer for higher Z, and static recrystallization would occur upon holding at temperature.

At lower strains, as in creep (32), a subgrain structure developed (Fig. 1) (36 50-56); the size was smaller for lower temperature and greater strain rate and strain (57). When this substructure is maintained to room temperature, the strength is increased about 50%, the effect is easier to achieve and is greater if the steel contains Nb (58). A substructure was observed in steel containing $Ni_3(AlTi)$ only when worked above the solution temperature (56).

Metal which has been worked in the dynamic recovery range will recrystallize when maintained at temperature; the rate being greater when the temperature is higher, the reduction greater and the initial grain size smaller (50 52 59). These results were confirmed by more precise measurement of the kinetics of recrystallization by Capeletti et al (42) using interrupted tensile tests and by Buhler, Bobbert and Rose (53) who used interrupted tensile tests, metallography and changes in preferred orientation (for Fe-18%Cr-11%Ni).

Polygonization during deformation was observed in Fe-36%Ni-10%Cr by Tamhankar, Plateau and Crussard (26 27). Fracture occurred by intergranular cracking since the grain boundaries did not migrate being pinned by precipitate particles.

The ductility of fully austenitic Fe-23%Cr-17%Ni was studied over a range of temperatures (5). The fracture strain, temperature and stress could be correlated by Eqn. 5 with $n' = 4.9$ and $Q = 80$ kcal/mol (335 kJ/mol) which differ from the constants for strength data $n' = 5.3$, $Q = 96$ kcal/mol (402 kJ/mol). This alloy shows increasing ductility with increasing strain rate. On the other hand Fe-26%Cr-10%Ni which is 10% δ ferrite has the same values of n' and Q for both fracture and strength correlations. Results for Fe-23%Cr-17%Ni appear in Fig. 4 .

The presence of δ ferrite in small quantities always lowers the ductility of austenite (1 5). For Fe-12%Cr examination of the ductility as a function of temperature showed that minima occur at 1025°C(1877°F) and at 1300°C(2372°F) due to two-phase regions of α/γ and γ/δ respectively (52). The temperature range of single phase austenite narrows as the chromium increases and the carbon decreases. In alloys containing δ ferrite minimum ductility occurs when the δ ferrite content is about 30%. Although the ductility rises with increasing percentage of δ ferrite, the possibility of over heating and melting increases (1). Ferrite may also be present as a result of segregation during casting. In alloys such as Fe-25%Cr-6%Ni, mixtures of ferrite and austenite can exhibit superplastic properties when they are in the microduplex structure (60). This structure, which is produced by hot rolling, consists of ferrite

and austenite grains about 3μm in diameter which are uniformly blended. Brittleness of the two phase structure can arise from the formation of chromium carbide at the interphase boundaries. These carbides can be avoided by lowering the carbon content or by adding Ti to form matrix carbides.

HOT WORKING OF SUPERALLOYS

Analysis of the data reviewed in the previous section shows a consistent behavior which is not affected substantially by major changes in composition. Since the compositions and microstructures of the superalloys are not greatly different from the above alloys under hot working conditions one could expect to find the same mechanisms. At the commencement of deformation (up to 50-80% reduction) the mechanism is dynamic recovery and subgrains form. If the deformation is continued to high strains, dynamic recrystallization will take place with the formation of equiaxed grains containing a variable substructure. Static recrystallization can take place after either mechanism if the working temperature is maintained. With increased solid solution alloying and in the presence of fine precipitates, the recrystallization either dynamic or static is delayed and slowed down. Grain boundary cracking is the usual mechanism of fracture; however its progress can be retarded and the ductility increased by the commencement of dynamic recrystallization. Coarse precipitates hasten fracture.

Review of the literature on the hot working of superalloys reveals that much of it is devoted to practical improvements in processing to achieve higher yields of more uniform and consistent product. The information concerning the mechanisms that can be gleaned from these publications will be summarized. There are only a few papers which have discussed the mechanisms to any extent.

The initial deformation causes strain hardening (61-63) and results in a structure which is not recrystallized (62 64-71) and which contains subgrains (72-75). The flow stress is of the order of 3 times that of low alloy steels and the rate of strain hardening is as high as that of an austenitic stainless steel (1). It is easier to observe the as-worked structure in cases where the deformation is below the ε or γ' solvus since the precipitates retard recrystallization (66 68 74 75). In Fig. 6, Oblak, Owczarski and Duvall (74) show that the substructure of Udimet 700 is stabilized by the presence of the precipitates as has been observed in TD Nickel (42) or Fe-18%Cr-10%Ni containing $Cr_{23}C_6$ (43). Because of the smaller amount of γ' during hot working, the substructure is quite different from that observed in aged metal after creep at lower temperatures (76). Retention of the hot worked substructure can improve the creep resistance at lower temperatures (73 75). Static recrystallization will result if cooling is delayed; the grain size is finer for deformation at lower temperatures, higher strain rates and greater reductions (1 68 70 77). Weiss, Grotke and Stickler (72) have observed static recrystallization nuclei growing into the hot-work substructure in Inconel 600.

Oblak and Owczarski (75) have developed the possibility of retaining the polygonized hot-worked substructure into a thermo-mechanical treatment for Udimet 700. Prior to hot working there is a 4 hr. solution anneal at 1171°C (2140°F) and a 4 hr. preliminary aging at 1066°C (1950°F) to precipitate the γ'. After working to a strain of 1.50 (78% reduction) there follows a further aging at 843°C (1550°F) for 4 hours and at 760°C (1400°F) for 16 hrs. The treatment greatly improves the room temperature mechanical properties and the creep resistance up to 760°C (1400°F). A treatment involving 60% reduction at 1010°C (1850°F) did give slightly inferior creep resistance to standard Udimet 700 at 704°C (1300°F) and above. In a thermo-mechanical treatment for Astroloy, mill annealed alloy was rolled to a 20% reduction at 843°C (1550°F). This refined the precipitate morphology giving better room

temperature properties but poorer creep resistance (67).

When the deformation is continued to high strains, the flow stress passes through a maximum and then decreases to a steady state regime. Shapiro, Muller and Dieter (61 62) have deformed Inconel 600 in torsion and have been able to observe the incidence of dynamic recrystallization after the peak. In general dynamic recrystallization is promoted by higher temperatures and higher strain rates. In hot torsion tests of Udimet 700 between 1060 and 1142°C (1940-2090°F), Young and Sherby (63)(Fig. 7) observed that the grains remain equiaxed and constant in size during steady state which is indicative of dynamic recrystallization. The microstructures observed after torsion were almost identical to those observed after extrusion at the same temperature, strain rate and strain. At higher working temperatures, the grain size was larger (62 63) and the γ' precipitate particles were fewer and larger but did not seem to have coalesced compared to undeformed specimens given the same thermal treatment. The occurrence of dynamic recrystallization in the presence of the γ' precipitate is somewhat surprising because Udimet 700 has been observed to resist recrystallization after rolling to a strain of 1.5 at 1065°C(1950°F)(74-75); however, in the latter case, the precipitates were finer, more numerous and more iniformly distributed.

The ductility is greatly improved if inclusions are eliminated, segregation reduced and the grain size reduced (1 5) Overheating before deformation can cause grain growth and increased dissolved alloy content which considerably reduces the ductility (70 72 77). Ductility of Udimet 700 was higher with the γ' precipitate than without because there was considerably less grain boundary sliding and cracking (74). The incidence of dynamic recrystallization inhibited propagation of grain boundary cracks and greatly raised the ductility of Inconel 600 in the manner described previously for simple nickel alloys (61 62).

Bailey (70 71) has conducted an extensive series of Gleeble tensile tests on Waspalloy, AL 718, and Udimet 625; similar tests have been carried out on Inconel 600 (72). In these tests as the temperature is raised, the ductility, measured by percent reduction in area at the neck, rises from a low value to a maximum and then decreases sharply as complete intergranular fracture occurs. The fracture at low temperatures (Udimet 700, 816-927°C (1500-1700°F); Waspalloy, 982°C (1800°F); and AL 718, 871°C (1600°F)) is partially intergranular and the worked material is at most slightly recrystallized. As the temperature rises, there is evidence of more recrystallization and the fracture mode becomes transgranular with considerable improvement in ductility. In Udimet 625, high ductility at 760°C (1400°F) and a transgranular fracture are associated with almost complete recrystallization. Since the inhibition of intergranular fracture in the intermediate temperature range is associated with observable recrystallization as in the hot torsion of Ni, Ni-Fe alloys, austenitic stainless steel and Inconel 600, it is concluded that in the Gleeble tests the recrystallization is dynamic and inhibits the propagation of grain boundary cracks. However, although optical metallography exposed the recrystallized grains, there was no transmission electron microscopy which could conclusively determine whether the new grains had been deformed or not; i.e., whether the recrystallization was dynamic or static. If the new grains are statically recrystallized, a new explanation for the inhibition of grain boundary fracture is needed.

The review of the literature shows that the mechanisms of dynamic recovery and recrystallization can account for the phenomena observed during hot forming of superalloys. However, it also is apparent that the processing of the age-hardenable superalloys involves many other steps subsequent to forming such as solution and precipitation of strengthening particles. Products with satisfactory properties can be manufactured only if attention is given to specifying each treatment as a part of the comprehensive procedure.

HOT COMPACTION OF SUPERALLOY POWDERS

The production of superalloy billets by compaction of prealloyed powders is important as a means of improving the workability by eliminating the segregation and columnar grain structure which is commonly found in cast ingots. It would appear to make possible the forming of certain alloys which after the most careful industrial casting practice cannot be worked at all. Satisfactory billets require prealloyed powder of precise composition, uncontaminated by oxidation and of suitable shape, size and size distribution. Facilities must be available for hot compacting the powder into billets without contamination from the environment. Cold pressing is unsatisfactory (78) because the high strength of the powder leads to such inadequate cold welding that the green strength is very low and limits the densification such that the shrinkage during sintering is unacceptable. Sintering without pressure which relies on surface and volume diffusion to enlarge the welds between the particles and to transport material into the voids (79 80 81) is too slow, and may result in non-uniform densification and poor dimensional control. What is needed is compaction at a temperature where the alloy has a much lower yield stress.

Hot pressing of the powder in a die (69) depends on several mechanisms. First, rapid deformation as in hot working and pressure welding when the force is initially applied. Second, a combination of dislocation creep and volume diffusion driven by both the applied stress (Nabarro-Herring microcreep) and by the surface energy (Kuczynski sintering) (69 80, 81). These latter mechanisms are very slow and tie up valuable press capacity. The dies are costly to prepare and maintain and present difficulties related to atmospheric control and dimensional retention. The compaction technique which gives satisfactory economic results is sealing the powder in an evacuated can succeeded by a normal hot forming process such as forging, extrusion or rolling (82-85). The mechanisms operative in this process are then pressure welding and the hot working mechanisms described earlier. The process has problems in prevention of contamination from the protective container and in removal of it.

Hot compaction has been shown to be technically successful. Billets and preforms have been produced which are free of contamination, possess much higher workability and exhibit considerably improved creep resistance (69 82-85). As a result of the very fine particle size achieved, superplastic deformation of IN 100 and Udimet 700 has been achieved with high ductility and reduced forming stress(84 85). To give the product satisfactory creep resistance, a 56 hour grain-coarsening treatment at 1245°C (2270°F) was necessary.

C O N C L U S I O N S

The hot working mechanisms of dynamic recovery and dynamic recrystallization function in the nickel-base superalloys as they do in the simple face-centered cubic alloys of iron, cobalt and nickel. The hot-worked substructure can give rise to subsequent static recrystallization which can be controlled to yield suitable grain sizes. Within a suitable sequence of thermomechanical treatments, the hot-worked structure can be retained to give improved mechanical properties including creep resistance.

REFERENCES

1. A.M. SABROFF, F.W. BOULGER and H.J. HENNING: Forging Materials and Practice, Reinhold, N.Y., 1968.

2. H.J. McQUEEN: J. Metals, 1968, 20, (4), 31-38.

3. W.J. McG. TEGART: Ductility, Am. Soc. Metals, Metals Park, Ohio, 1968, 133-77.

4. J.J. JONAS, C.M. SELLARS and W.J. McG. TEGART: Met. Rev., 1969, 14, 1-24.

5. C.M. SELLARS and W.J. McG. TEGART: Int. Met. Rev., 1971, 17, 1-24.

6. H.J. McQUEEN and W.J. McG. TEGART: Scientific American, 1973, submitted.

7. H.J. HENNING and F.W. BOULGER: Mechanical Working of Steel I, Gordon and Breach, N.Y., 1964, 107-125.

8. H.J. McQUEEN and J.J. JONAS: Metal Forming: Interrelation Between Theory and Practice, Plenum, N.Y., 1971, 393-428.

9. J.J. JONAS, H.J. McQUEEN, and W.A. WONG: Deformation Under Hot Working Conditions (SP 108), Iron Steel Inst., London, 1968, 49-59.

10. H.J. McQUEEN, W.A. WONG and J.J. JONAS: Can. J. Phys., 1967, 45, 1225-35.

11. W.A. WONG and J.J. JONAS: Trans. TMS-AIME, 1968, 242, 2271-80.

12. H.J. McQUEEN and J.E. HOCKETT: Met. Trans., 1970, 1, 2997-3004.

13. J.E. HOCKETT and H.J. McQUEEN: Proc. 2nd. Int. Conf. Strength of Metals and Alloys (Asilomar, 1970), ASM, Metals Park, 991-95.

14. D.J. ABSON and J.J. JONAS: Met., Sci., J., 1970, 4, 24-28.

15. W.A. WOOD and J.W. SUITER: J. Inst.Met., 1951-52, 80, 501.

16. M.G. LOZINSKII, V.S. MIROTVORKII and E.I. ANTIPOVA: Metal Science and Heat Treatment of Metals, 1963, (56), 294-99.

17. H.J. McQUEEN: Trans. Japan Inst. Metals, 1968, 9 Sup., 170-77.

18. K.J. IRVINE, T. GLADMAN, J. ORRAND, F.B. PICKERING: J. Iron Steel Inst., 1970, 208, 717-26.

19. J.D. BAIRD, R.R. PRESTON: Hot Workability of Steel, Iron Steel Inst., London, 1969.

20. W.J. McG. TEGART: Metals Australia, 1971, 3, (1), 3-8.

21. D. HARDWICK and W.J. McG. TEGART: J. Inst. Metals, 1961-62, 90, 17-20.

22. C.M. SELLARS and W.J. McG. TEGART: Acta Met., 1966, 14, 1136-38.

23. H.J. McQUEEN and S. BERGERSON: Met. Sci. J., 1972, 6, 25-29.

24. R.A.P. DJAIC and J.J. JONAS: J. Iron Steel Inst., 1972, 210, 256-61.

25. R.A.P. DJAIC and J.J. JONAS: Met. Trans., (in press).

26. C. CRUSSARD and R. TAMHANKAR: Trans. AIME, 1958, 212, 718-30.

27. R. TAMHANKAR, J. PLATEAU and C. CRUSSARD: Rev. Mét., 1958, 55, 383-400.

28. A.GITTINS: Fracture of Metals Under Hot Working Conditions, Rep. 29/1, BHP Res. Lab., Melbourne, 1970.

29. E. SHAPIRO and G.E. DIETER: Met. Trans., 1971, 2; 1385-91.

30. F.E. WHITE and C. ROSSARD: Deformation Under Hot Working Conditions (SP 108), Iron Steel Inst., London, 1968, 14-20.

31. M.J. LUTON and W.J. McG. TEGART: Met. Sci.J., 1969, 3, 142-46.

32. F. GAROFALO, C. RICHMOND, W.F. DOMIS and F. von GEMMINGEN: Joint Int. Conf. on Creep, Inst. Mech. Engin., London, 1963,I31-39.

33. J.L. ROBBINS, O.C. SHEPARD and O.D. SHERBY: J. Iron Steel Inst., 1961, 199, 175-80.

34. J.L. ROBBINS, O.C. SHEPARD and O.D. SHERBY: Trans. ASM, 1967, 60, 205-16.

35. R.A. REYNOLDS and W.J. McG. TEGART: J. Iron Steel Inst., 1962, 200,1044-59.

36. C. ROSSARD: Métaux Corros. Inds., 1960, 35; 102-15, 140-53, 190-205.

37. S. GORCZYCA: Mém. Scient. Rev. Méts., 1960, 57, 153-58.

38. A.P. GULYAYEV and A.S. SHIGAREV: Phys. Metals Metallog., 1964, 18, (2), 73-79.

39. H. OHMORI: Trans. Japan Inst. Metals, 1966, 7, 153-57.

40. R.F. DEWSNAP: J. Iron Steel Inst., 1970, 208, 727-43.

41. G.A. WILBER, J.R. BELL, J.H. BUCHER and W.J. CHILDS: Trans. TMS-AIME, 1968, 242,2305-08.

42. T.L. CAPELETTI, L.A. JACKMAN, W.J. CHILDS: Met. Trans., 1972, 3, 789-96.

43. A.H. CLAUER and B. WILCOX: Met. Sci. J., 1967, 1, 86-90.

44. S.R. KEOWN and F.B. PICKERING: Effect of $Cr_{23}C_6$ on Creep Strength and Ductility of Austenitic Steels (PM 5281/4/68/A), United Steel Co., England, 1968.

45. J. DAUVERGNE, M. PELABON and J. IVERNEL: Rev. Mét., 1954, 51, 254-64.

46. J.M. JAQUERIE and L. HABRAKEN: Cobalt, 1968, 38, 13-19.

47. M.J. LUTON and C.M. SELLARS: Acta Met., 1969, 17, 1033-43.

48. B. DRUBE and H.P. STUWE: Z. Metallk., 1967, 58, 799-804.

49. J.P. SAH, G.J. RICHARDSON and C.M. SELLARS: J. Aust. Inst. Metals, 1969, 14, 292-97.

50. J. PLUHAR and P. ZUNA: J. Iron Steel Inst., 1969, 207, 58-62.

51. S.R. KEOWN: Microh, 1969, 1, 120-48.

52. A. GUEUSSIER and R. CASTRO: Rev. Mét., 1958, 55, 1023-40.

53. H. BUHLER, D. BOBBERT and A. ROSE: Stahl u. Eisen, 1970, 90, 21-28.

54. H.J. McQUEEN, H. WEISS and L. NORTHWAY: Private Communication, BHP Melbourne Research Lab., Australia.

55. Ye. N. SOKOLKOV and Yu. P. SURKOV: Phys. Metals Metallog. 1963, 16, (6), 107-09.

56. R.S. SHKLYAR, et al: ibid, 1966, 21, (1), 47-52.

57. Ye. N. SOKOLKOV, Yu. P. SURKOV and D.I. GURFEL: ibid., 1965, 20, (4), 83-88.

58. K.J. IRVINE, T. GLADMAN and F.B. PICKERING: J. Iron Steel Inst., 1969, 207, 1017-28.

59. R. WUSATOWSKI: J. Iron Steel Inst., 1966, 204, 727-36.

60. H.W. HAYDEN, R.C. GIBSON, H.F. MERRICK and J.H. BROPHY: ASM Trans. Q. 1967, 60, 3-14; 1968, 61, 85-93.

61. G.E. DIETER, J.V. MULLIN and E. SHAPIRO: Deformation Under Hot Working Conditions (SP 108), Iron Steel Inst., London, 1968, 7-13.

62. E. SHAPIRO and G.E. DIETER: Met. Trans. 1970, 1, 1711-19.

63. C. M.YOUNG and O.D. SHERBY: Simulation of Hot Forming Operations by Means of Hot Torsion, AFML-TR-69-294, Stanford Univ., Palo Alto, 1969.

64. J.B. BARBER: Report, H. Wiggin Co., Hereford, U.K.

65. M.J. DONACHIE, A.A. PINKOWISH, W.P. DONESI, J.F. RADAVICH and W.H. COUTS, Met. Trans., 1970, 1, 2623-30.

66. R.S. CREMISIO, H.M. BUTLER and J.F. RADAVICH: J. Metals, 1969, 21, (11), 55-61.

67. R.K. HOTZLER, R.J. MacIAG, G.J. FISHER and E. TROC: Met. Trans., 1970, 1, 963-67.

68. A.J. De RIDDER and R.J. NOEL: SAE Publication Paper 690 101, 1969.

69. M.M. ALLEN, R.L. ATHEY and J.B. MOORE: Met. Eng. Q., 1970, 10, (1), 20-30.

70. R.E. BAILEY: Microstructural Examination of Waspaloy and AL-718 Gleeble Hot Workability Test Specimens (Report SP-69-9), Allegheny Ludlum Steel Corp., Research Center, Brackenridge, Pa., 1969.

71. R.E. BAILEY: Hot Working Behavior of Wrought Udimet 625 As Characterized by Gleeble Testing (Report SP-70-11), Special Metals Corp. Research Department, New Hartford, N.Y., 1970.

72. B. WEISS, G.E. GROTKE and R. STICKLER: Welding Res. Sup., 1970, 35, 471S-487S.

73. V.D. SADOVSKY et al: Phys. Metals Metallog., 1964, 17, (6), 47-53.

74. J.M. OBLAK, W.A. OWCZARSKI and D.S. DUVALL: Met. Trans. 1971, 2, 1499-1501.

75. J.M. OBLAK and W.A. OWCZARSKI: ibid., 1972, 3, 617-26.

76. G.R. LEVERANT and B.H. KEAR: ibid., 1970, 1, 491-98.

77. R.S. CREMISIO: Trans. Vac. Met. Conf., 1965, 75-97.

78. E.V. KELLEY and R.H. DYER: Metal Progress, 1972, 101 (4), 53-58.

79. F. THUMMLER and W. THOMMA: Met. Rev., 1967, 12, 69-108.

80. F.V. LENEL and G.S. ANSELL: Modern Developments in Powder Metallurgy, Vol.1, Plenum, New York, 1966, 281-96.

81. R.L. COBLE: Fundamental Phenomena in the Materials Science, Vol. 1: Sintering and Plastic Deformation, Plenum, N.Y., 1964, 11-23.

82. G. FRIEDMAN and E. KOSINSKI: Met. Eng. Q., 1971, 11 (1), 48-50.

83. J.C. FRECHE, W.J. WATERS and R.L. ASHBROOK: ibid., 1970, 10 (2), 58-59.

84. S.H. REECHMAN, B.W. CASTLEDINE and J.W. SMYTHIE: Superalloy P/M Components for Elevated Temperature Applications (Preprint 700 140), SAE, N.Y., 1970.

85. S.H. REICHMAN and J.W. SMYTHIE: Int. J. Powder Met., 1970, 6, (1), 65.

FIG. 1 Hot worked microstructures as observed by transmission electron microscopy of thin foils. (a) Dynamic recovery substructure in 18%Cr-8%Ni austenitic steel which has been deformed in hot torsion at 1000°C (1832°F) and 0.68 s^{-1} to a strain of 1.11 (54). (b) Statically recrystallized nuclei are growing into the dynamically recovered substructure in Cu which has been rolled at 600°C (1112°F) and 20 s^{-1} to a strain of 2.2. The specimen was quenched in 0.1 s after leaving the rolls (17). (c) Substructure in dynamically recrystallized Cu which has been twisted at 800°C (1472°F) and 11.1 s^{-1} to a strain of approximately 30. The specimen was quenched during deformation to prevent static recrystallization (23).

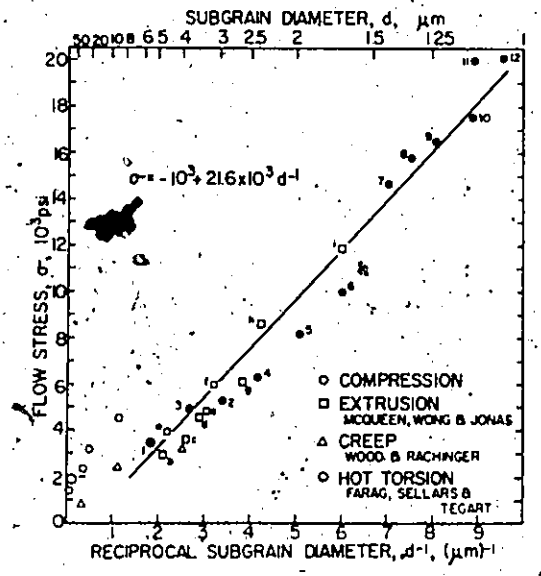

FIG. 2 The relationship between the steady state flow stress of aluminum and the equilibrium substructure which has developed during the deformation (12).

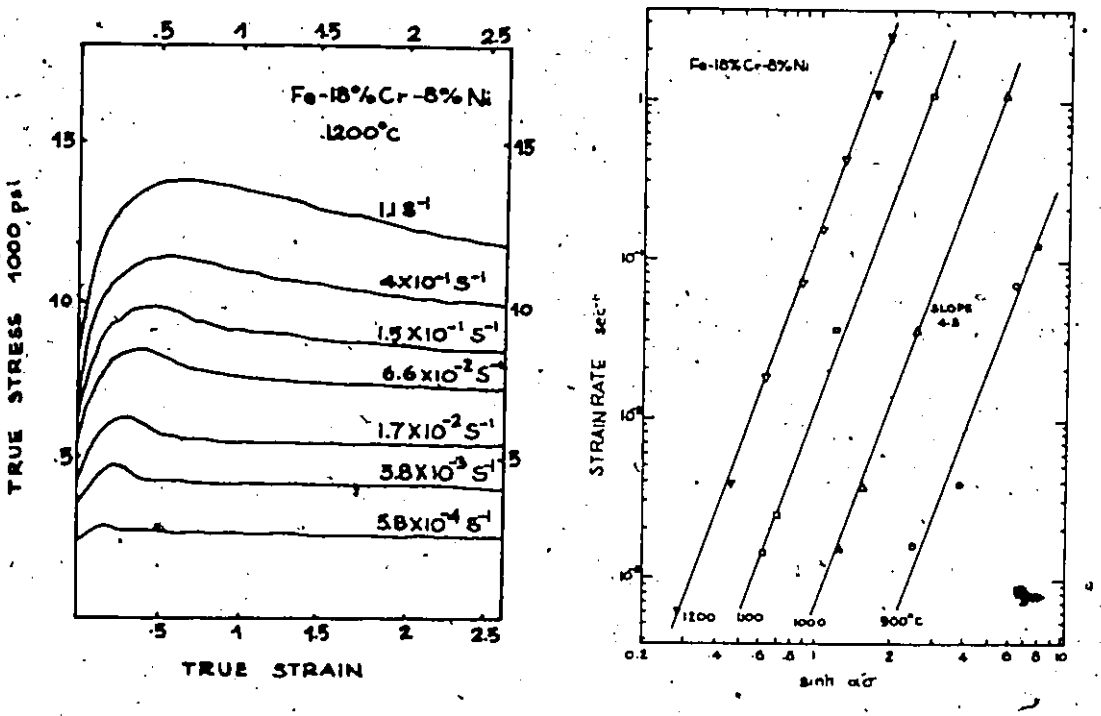

FIG. 3 Flow curves exhibiting steady state deformation in which the parameters can be correlated by the hyperbolic sine formula. (a) Effective stress - effective strain curves of austenitic stainless steel at 1200°C (2192°F) (36). The curves are characteristic of metals in which dynamic recrystallization begins at the peak. The continual decrease at high strain rates is the result of partial adiabatic heating. (b) The strain rate, temperature and steady state flow stress of austenitic stainless steel are correlated according to Eqn.2 with the constants

$Q = 97$ k cal/mol (405kJ/mol) $\quad \alpha = 9.27 \times 10^{-5}$ $(psi)^{-1}$ and $\quad n' = 4.30$

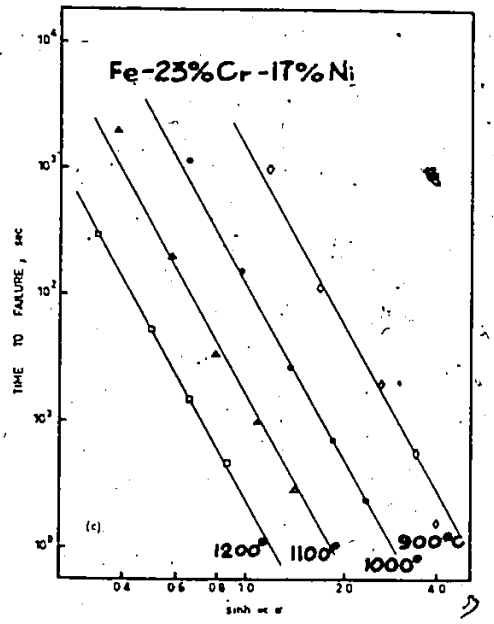

FIG. 4 The time to rupture can be correlated with the deformation conditions by Eqn. 5. This data is taken from hot torsion tests on fully austenitic stainless steel Fe-23%Cr-17%Ni (5).

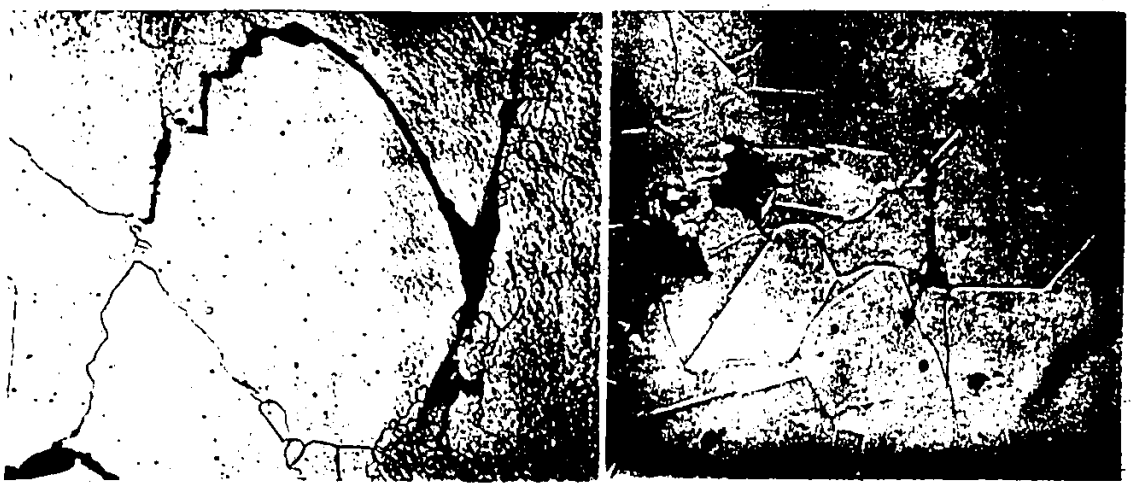

FIG. 5 Grain boundary cracking in Ni-5%Fe deformed at a strain rate of 2×10^{-3} s^{-1}. (a) At 760°C (1400°F) the cracks propagate (ε=0.35). × 125. (b) At 934°C (1710°F) dynamic recrystallization has prevented propagation (ε=1.6). × 625. (31).

FIG. 6 This transmission electron micrograph illustrates the substructure present in thermomechanically treated Udimet 700. The specimen was aged to precipitate γ' and was then swaged at 1950°F to a reduction of 78% (74).

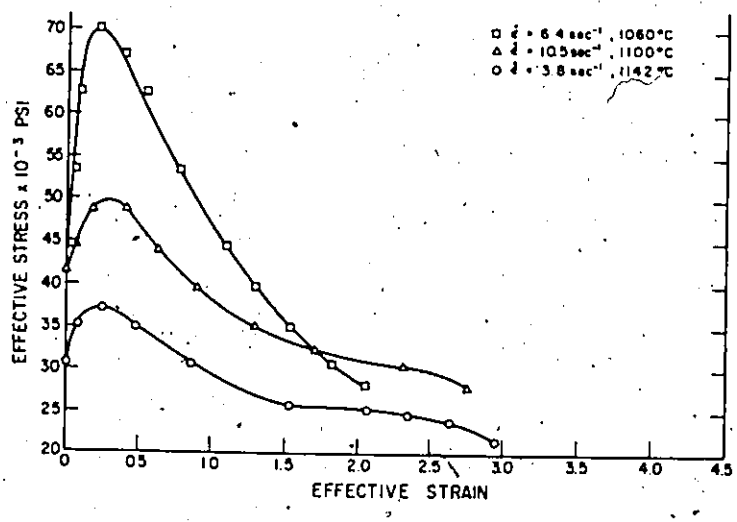

FIG. 7 Effective stress-effective strain curves from hot torsion tests on Udimet 700. The tests were not continued to fracture but interrupted at the strains shown so that the microstructures could be compared with those of extrusions produced under the same conditions. The rise in flow stress is the result of hardening during dynamic recovery and the drop is the result of dynamic recrystallization (63).